Colloquium: Roper resonance: Toward a solution to the fifty year puzzle

Volker D. Burkert*

Thomas Jefferson National Accelerator Facility, Newport News, Virginia 23606, USA

Craig D. Roberts†

Physics Division, Argonne National Laboratory, Argonne, Illinois 60439, USA

(published 14 March 2019)

Discovered in 1963, the Roper resonance appears to be an exact copy of the proton *except* that its mass is 50% greater and it is unstable. These features of the Roper have been very difficult to explain so that for half a century this lightest excited state of the proton has defied understanding. The last decade has presented a new challenge, viz. precise information on the proton-to-Roper electroproduction transition form factors. Reaching to momentum transfer $Q^2 \approx 4.5$ GeV^2, the data probe a domain within which hard valence-quark degrees of freedom could be expected to determine form factor behavior. An explanation of the Roper should combine an understanding of all these things. This is a prodigious task, but a ten-year international collaborative effort, involving experimentalists and theorists, has presented a candidate solution to the puzzle. Namely, the observed Roper is at the heart of the proton's first radial excitation, consisting of a dressed-quark core augmented by a meson cloud that reduces the core mass by approximately 20% and materially alters its electroproduction form factors on $Q^2 < 2m_N^2$, where m_N is the proton's mass. This Colloquium describes the experimental developments which enabled electroproduction data to be procured within a domain that is the purview of strong quantum chromodynamics, thereby providing challenges and opportunities for modern theory, and surveys the developments in reaction models and QCD theory that have enabled this picture of the Roper resonance to be drawn.

DOI: 10.1103/RevModPhys.91.011003

CONTENTS

I. INTRODUCTION

The hydrogen atom played a crucial role in the development of the modern approach to fundamental interactions, but it required more than merely knowledge of the ground state to spur the breakthroughs. A chart of the hydrogen atom spectrum, i.e., the excited states, was necessary to validate the jump to quantum mechanics via the Bohr model (Bohr, 1913), and the discovery of the Lamb shift between the $2S_{1/2}$ and $2P_{1/2}$ levels within that spectrum (Lamb and Retherford, 1947) was critical to forcing the steps from the Dirac equation (Dirac, 1928) to quantum electrodynamics (QED) (Feynman, 1966; Tomonaga, 1966; Schwinger, 1982).

The same has been true in the development of quantum chromodynamics (QCD), the strong interaction piece of the standard model of particle physics, which emerged more than forty years ago from an array of distinct ideas and discoveries (Marciano and Pagels, 1978, 1979). Owing to the existence of three readily accessible "flavors" of lighter quarks, the spectrum of ground-state strongly interacting particles (hadrons) revealed a great deal, leading to the quark model (Gell-Mann, 1964; Zweig, 1964) with its wide range of successful predictions. However, the first excited state of the proton did not fit the standard picture. This state, the Roper resonance, was discovered in 1963 (Adelman, 1964; Auvil *et al.*, 1964; Bareyre *et al.*, 1964; Roper, 1964; Roper, Wright, and Feld, 1965), and its characteristics have been the source of great puzzlement since that time.

The Roper is the lightest excitation of the proton, and the proton is arguably the most fundamental bound state in nature, being simultaneously the first hadron and the first nucleus discovered (Geiger and Marsden, 1909; Rutherford, 1911), and seemingly absolutely stable (Tanabashi *et al.*, 2018). The Roper is therefore a benchmark, and no claim that the standard model is understood can be sustained until a resolution is found to the

*burkert@jlab.org
†cdroberts@anl.gov

mystery that surrounds the nature of this first excited state of the proton.

We begin, therefore, with a statement of the Roper's simplest characteristics: it is a $J = 1/2$ positive-parity resonance with pole mass ≈1.37 GeV and width ≈0.18 GeV (Tanabashi *et al.*, 2018). In the spectrum of nucleonlike states, i.e., baryons with isospin[1] $I = 1/2$, the Roper resonance lies about 0.4 GeV above the ground-state nucleon and 0.15 GeV below the first $J = 1/2$ negative-parity state, which has roughly the same width. Today, the levels in this spectrum are labeled $N(\text{mass})J^P$. Hence, the ground-state nucleon is denoted as $N(940)1/2^+$, the Roper resonance as $N(1440)1/2^+$, and the negative-parity state previously described is $N(1535)1/2^-$.

The search for an understanding of the Roper resonance is the highest profile case in a long-running effort to chart and explain the spectrum and interactions of strong interaction bound states. The importance of this effort has long been recognized. Indeed, baryons and their resonances play a central role in the existence of our Universe and ourselves; and therefore (Isgur, 2000) "… they must be at the center of any discussion of why the world we actually experience has the character it does. I am convinced that completing this chapter in the history of science will be one of the most interesting and fruitful areas of physics for at least the next thirty years."

QCD, which should describe all hadrons and, ultimately, the properties of every atomic nucleus, is the theory of gluons (gauge fields) and quarks (matter fields). It is conceptually simple and can be expressed compactly in just one line, with two definitions (Wilczek, 2000). And yet, nearly four decades after its formulation, we are still seeking answers to such apparently simple questions as what is the proton's wave function and which, if any, of the known baryons is the proton's first radial excitation? Numerous problems remain open because QCD is fundamentally different from the standard model's other pieces: while a perturbation theory exists and is a powerful tool when used in connection with high-energy QCD processes, it is essentially useless when it comes to developing an understanding of strong interaction bound states built from light quarks.

The study of light-hadron properties is a problem in strong QCD (sQCD), viz. the body of experimental and theoretical methods used to probe and map the infrared domain of standard model physics. Here emergent phenomena, such as gluon and quark confinement and dynamical chiral symmetry breaking (DCSB), play the dominant role in determining all observables of the theory. The nature of sQCD and its contemporary methods and challenges will become apparent as we recount the history of the Roper resonance and the recent developments which have enabled a coherent picture of this system to emerge and, by analogy, an array of related resonances.

[1]Isospin is a quantum number associated with strong interaction bound states. Its value indicates the number of electric-charge states that may be considered as (nearly) identical in the absence of electroweak interactions, e.g., the neutron and proton form an $I = 1/2$ multiplet and are collectively described as nucleons.

II. CONSTITUENT-QUARK MODEL EXPECTATIONS

Theoretical speculations on the nature of the Roper resonance followed immediately upon its discovery. For instance, it was emphasized that the enhancement observed in experiment need not necessarily be identified with a resonant state (Dalitz and Moorhouse, 1965), but if it is a resonance, then it has structural similarities with the ground-state nucleon (Moorhouse, 1966).

The Roper was found during a dramatic period in the development of hadron physics, which saw the appearance of "color" as a quantum number carried by "constituent quarks" (Greenberg, 1964), the interpretation of baryons as bound states of three such constituents (Gell-Mann, 1964; Zweig, 1964), and the development of nonrelativistic quantum mechanical models with two-body potentials between constituent quarks that were tuned to describe the baryon spectrum as it was then known (Hey and Kelly, 1983). Owing to their mathematical properties, harmonic oscillator potentials were favored as the zeroth-order term in the associated Hamiltonian:

$$H_0 = T + U_0, \qquad T = \sum_{i=1}^{3} \frac{p_i^2}{2M_i}, \qquad U_0 = \sum_{i<j=1}^{3} \frac{1}{2} K r_{ij}^2, \tag{2.1}$$

where p_i are the constituent-quark momenta, r_{ij} are the associated two-body separations, and spin-dependent interactions were treated as (perturbative) corrections. The indices in Eq. (2.1) sample the baryon's constituent-quark flavors so that, e.g., in the proton, $\{1,2,3\} \equiv \{U = \text{up}, U = \text{up}, D = \text{down}\}$, and K is a common "spring constant" for all the constituents. If one assumes that all three constituent quarks have the same mass, viz. $M_1 = M_2 = M_3$, then this Hamiltonian produces the level ordering in Fig. 1. [A similar ordering of these

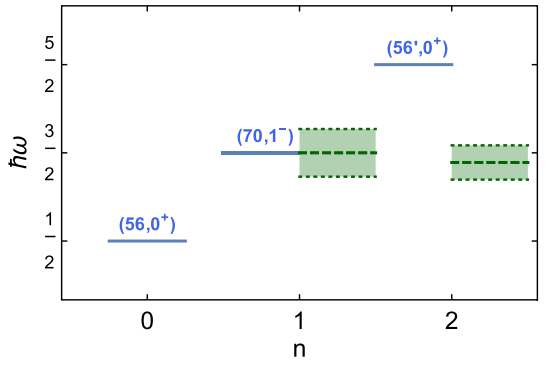

FIG. 1. Solid blue lines: level ordering produced by the Hamiltonian in Eq. (2.1). The $(56', 0^+)$ level represents a supermultiplet that is completed by the states in the following representations of $SU(3) \times O(3)$: $(56, 2^+)$, $(20, 1^+)$, $(70, 2^+)$, and $(70, 0^+)$. Dashed green lines and shaded bands: pole mass and width of the nucleon's two lowest-lying $J = 1/2$ excitations, determined in a wide ranging analysis of available data (Kamano *et al.*, 2013). For the purposes of this illustration, $\hbar\omega$ is chosen so that the proton-$N(1535)1/2^-$ splitting associates the $N(1535)1/2^-$ state with the $(70, 1^-)$ supermultiplet, as suggested in quantum mechanics by its spin and parity.

low-lying levels is also obtained with linear two-body potentials (Richard, 1992).]

It is evident in Fig. 1 that the natural level ordering obtained with such potential models has the first negative-parity $\Delta L = 1$ angular momentum excitation of the ground-state three-quark system—the $N(1535)1/2^-$— at a lower energy than its first radial excitation. If the Roper resonance $N(1440)1/2^+$ is identified with that radial excitation, whose quantum numbers it shares, then there is immediately a serious conflict between experiment and theory. However, this ignores the "perturbations," i.e., corrections to H_0, which might describe spin-spin, spin-orbit, and other kindred interactions that can eliminate the degeneracies in $n \geq 2$ harmonic oscillator supermultiplets. (There are no such degeneracies in the $n = 0$, 1 supermultiplets.) It was subsequently proved (Gromes and Stamatescu, 1976; Isgur and Karl, 1979) that given any anharmonic perturbation of the form $\sum_{i<j} U(r_{ij})$, then at first order in perturbation theory the $n = 2$ supermultiplet is always split as depicted in Fig. 2, where Δ is a measure of the shape of the potential. In practice, there is always a value of Δ for which the $(56', 0^+)$ (Roper) state is shifted below the $N(1535)1/2^-$. Typically, however, the value is so large that one must question the validity of first-order perturbation theory (Isgur and Karl, 1979).

Notwithstanding such difficulties, at this time it was not uncommon for practitioners to imagine that such models were providing a realistic picture of the baryon spectrum and, in fact, they were a *phenomenal phenomenological success* (Hey and Kelly, 1983). Such conclusions were premature as made clear by Sec. III herein and also the vast array of novel experimental results from the Belle, *BABAR*, BESIII, and LHCb Collaborations (Aaij *et al.*, 2015; Braaten, 2016; Shen, 2016), which reveal states that cannot be explained by quark models.

This period of enthusiasm coincided with the "discovery" of QCD (Marciano and Pagels, 1978, 1979). Some of its peculiar features had been exposed on the perturbative domain (Gross, 2005; Politzer, 2005; Wilczek, 2005), but the spectrum of bound states it supported could not then be determined. (It may still be said today that the complete spectrum of bound states supported by real QCD, i.e., in the presence of dynamical quarks with realistic values for their current masses, is unknown.)

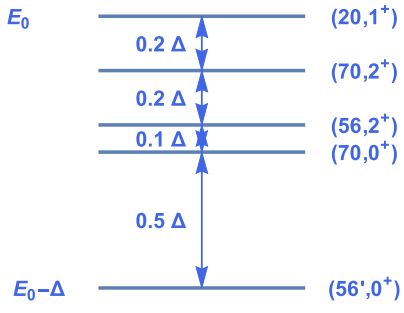

FIG. 2. If an arbitrary anharmonic potential, restricted only insofar as it can be written as a sum of two-body terms, is added to H_0 in Eq. (2.1), then at first order in perturbation theory the $n = 2$ harmonic oscillator supermultiplet is split as indicated here. [E_0 is roughly the original $(56', 0^+)$ energy and Δ is a measure of the shape of the potential.]

In the absence of approaches with a direct QCD connection, studies of quantum mechanical constituent-quark models (CQMs) continued. In relation to the Roper resonance it was found that within a broad class of phenomenological potentials, the negative-parity orbital excitation of the three-quark ground state is always lighter than the $L = 0$ radial excitation (Høgaasen and Richard, 1983; Richard, 1992). This means that the ordering in Fig. 2 is an artifact of first-order perturbation theory, which is unreliable when the leading correction is comparable to the value of $\hbar\omega$ associated with H_0, and, moreover, that the ordering of the nucleon's low-lying excitations is incorrect in a wide array of such constituent-quark models (Capstick and Roberts, 2000; Crede and Roberts, 2013; Giannini and Santopinto, 2015).

The difficulty in providing a sound theoretical explanation of the Roper resonance was now becoming apparent. In fact, at this point it was considered plausible that the $N(1440)1/2^+$ might not actually be a state generated by three valence quarks. It was also conjectured that the Roper might be a breathing mode of the ground-state nucleon, if the latter is realized as a topological soliton (Kaulfuss and Meissner, 1985; Mattis and Karliner, 1985). And the notion was also entertained that it may be a hybrid, viz. a system with a material valence-gluon component or, at least, that the Roper might contain a substantial hybrid component (Barnes and Close, 1983; Li, Burkert, and Li, 1992; Capstick and Page, 2002).

The appearance of QCD refocused attention on some prominent weaknesses in the formulation of CQMs. In particular, their treatment of constituent-quark motion within a hadron as nonrelativistic, when calculations showed $\langle p_i \rangle \sim M_i$, where $\langle p_i \rangle$ is the mean momentum of a bound constituent quark, and the use of nonrelativistic dynamics, e.g., the omission of calculable relativistic corrections to the various potential terms, which would normally become energy dependent. Consequently, a relativized constituent-quark model was developed (Godfrey and Isgur, 1985) and applied to the baryon spectrum (Capstick and Isgur, 1986). But these improvements did not change the ordering of the energy levels, i.e., the low-lying excitations of the nucleon were still ordered as depicted in Fig. 1. This remains true even within a relativistic field theory framework that employs instantaneous interquark interactions to compute the baryon spectrum (Löring, Metsch, and Petry, 2001), namely, a three-body term expressing linear confinement of constituent quarks and a spin-flavor-dependent two-body interaction to describe spin-dependent mass splittings.

The QCD-inspired CQMs described above all assume that interquark dynamics derives primarily from gluon-related effects. An alternative is to suppose that the hyperfine interaction between constituent quarks is produced by exchange of the lightest pseudoscalar mesons (Glozman and Riska, 1996), i.e., the pseudo–Nambu-Goldstone modes: π, K, and η mesons, in which case the hyperfine interaction is flavor dependent in contrast to that inferred from one-gluon exchange. Using algebraic arguments, one may demonstrate that this sort of Goldstone boson-exchange (GBE) hyperfine interaction produces more attraction in systems whose wave

functions possess higher spin-flavor symmetry. Such dynamics can thus lead to an inversion of the excited state levels depicted in Fig. 1, so that the Roper resonance, viewed as the lowest radial excitation of a three constituent-quark ground state, lies below the $N(1535)1/2^-$, the first orbital excitation of that system. This inversion of levels is a positive feature of the model, and it hints that mesonlike correlations should play a role in positioning states in the baryon spectrum. [Similar conclusions may be drawn from analyses of unquenched CQMs (Julia-Diaz and Riska, 2006).]

On the other hand, a GBE picture of baryon structure can be only figurative at best. All mesons are composite systems with radii that are similar in magnitude to those of baryons, and hence one-boson exchange between constituent quarks cannot be understood literally (Chen *et al.*, 2018). A deeper class of questions is relevant to all such CQMs. Namely, in the era of QCD can any connection be drawn between that underlying theory and the concept of a constituent quark? Can the interactions between the lightest quarks in nature veraciously be described by a potential of any kind? And notwithstanding the challenges they face in describing the Roper resonance, do their apparent successes in other areas yield any sound insights into strong interaction phenomena? At present, each practitioner has their own answers to these questions. Our view is that CQMs continue to be a valuable part of the sQCD toolkit.

III. ROPER RESONANCE IN EXPERIMENT

A. Sparse data

One source of the difficulty in understanding the Roper resonance is the quality of the data that was available in the previous millennium. Illustrated by Fig. 3, it was poor owing to limitations in sensitivity to the channels $\gamma p \to \pi^0 p$ and $ep \to e\pi^0 p$ that were typically employed in analyses of the photocoupling and electrocoupling helicity amplitudes and transition form factors. Such data could not reasonably be used to distinguish between competing theoretical models of the Roper resonance. It was thus evident, given that physics is an empirical science, that a key to resolving the conundrum was more and better data, i.e., to replace the limited data available in the previous millennium with a much larger set of high-precision data. This was strong motivation for a new experimental program at what is now known as the Thomas Jefferson National Accelerator Facility (JLab), which began operations in 1994 and was then called the Continuous Electron Beam Accelerator Facility (CEBAF).

B. Electroproduction kinematics

The data in Fig. 3 were obtained in single-pion photoproduction and electroproduction processes $eN \to e\pi N$. The production of a $J = 1/2^+$ resonance in the intermediate part of such reactions is described by an electromagnetic current that is completely expressed by two form factors:

$$\bar{u}_f(P_f)\left[\gamma_\mu^T F_1^*(Q^2) + \frac{1}{m_{fi}}\sigma_{\mu\nu}Q_\nu F_2^*(Q^2)\right]u_i(P_i), \qquad (3.1)$$

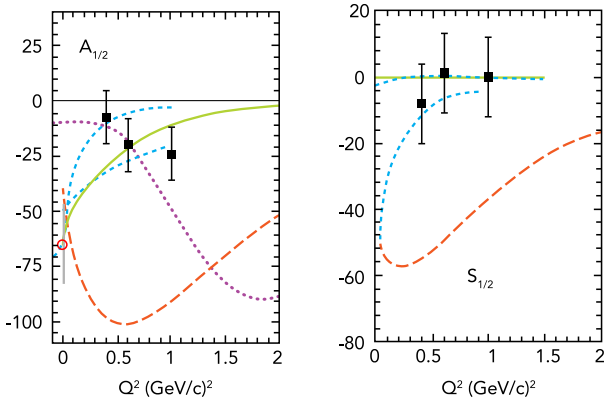

FIG. 3. Data on the (left panel) transverse and (right panel) longitudinal Roper resonance photo- and electrocoupling helicity amplitudes, Eqs. (3.2), as they were available in the last millennium. Data: open (red) circle—1998 estimate of $A_{1/2}$ at the photoproduction point (Caso *et al.*, 1998), and error bar (gray)—our assessment of the true uncertainty in this value at that time. Solid squares and short-dashed (cyan) curves—results from a fixed-t dispersion relation fit (Gerhardt, 1980), where the error bars on the squares are our estimate of the systematic uncertainty. Model results: long-dashed (red) curves—nonrelativistic quark model (Koniuk and Isgur, 1980; Close and Li, 1990) (incompatible with then-existing data); dotted curve (purple, left panel)—relativized quark model (Warns *et al.*, 1990); and solid curve (green)—model constructed assuming the Roper is a hybrid system, constituted from three constituent quarks plus a type of gluon excitation (Li, Burkert, and Li, 1992), wherewith the longitudinal amplitude vanishes. Ordinate expressed in units of 10^{-3} GeV$^{-1/2}$.

where u_i and $\bar{u}_f$ are, respectively, Dirac spinors describing the incoming or outgoing baryons, with four-momenta $P_{i,f}$ and masses $m_{i,f}$ so that $P_{i,f}^2 = -m_{i,f}^2$, $Q = P_f - P_i$, $m_{fi} = m_f + m_i$, and $\gamma^T \cdot Q = 0$. In terms of these quantities, the helicity amplitudes in Fig. 3 are

$$A_{1/2}(Q^2) = c(Q^2)[F_1^*(Q^2) + F_2^*(Q^2)], \qquad (3.2a)$$

$$S_{1/2}(Q^2) = \frac{|\mathbf{q}|}{\sqrt{2}}c(Q^2)\left[F_1^*(Q^2)\frac{m_{fi}}{Q^2} - \frac{F_2^*(Q^2)}{m_{fi}}\right], \qquad (3.2b)$$

with $Q_\pm^2 = Q^2 + (m_f \pm m_i)^2$, $K = (m_f^2 - m_i^2)/(2m_f)$,

$$c(Q^2) = \left[\frac{\alpha_{\rm em}\pi Q_-^2}{m_f m_i K}\right]^{1/2}, \qquad |\mathbf{q}| = \frac{\sqrt{Q_-^2 Q_+^2}}{2m_f}, \qquad (3.3)$$

where $|\mathbf{q}|$ is the magnitude of the virtual-photon three-momentum in the resonance rest frame.

The dominant Roper decay is $N(1440) \to N\pi$, where the neutron $+ \pi^+$ $(n\pi^+)$ channel is most prominent. It also couples to the two-pion channel, being there most conspicuous in $N(1440) \to p\pi^+\pi^-$, where p labels the proton. By design, the CEBAF Large Acceptance Spectrometer (CLAS) at JLab was ideally suited to measuring both these reactions in the same experiment, simultaneously employing the polarized high-precision continuous-wave electron beam at energies up

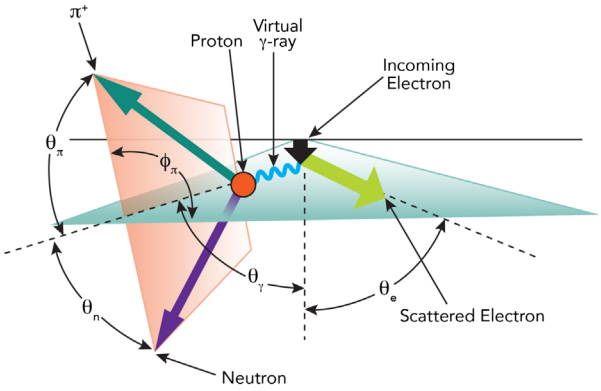

FIG. 4. Kinematics of π^+ electroproduction from a proton.

to 6 GeV. This capability provided the CLAS Collaboration with a considerable advantage over earlier experiments because measurements and extractions of Roper resonance observables could be based on the analysis of complete center-of-mass angular distributions and large energy range, and cross checked against each other in different channels.

A typical kinematics choice for the reaction $ep \to en\pi^+$ is depicted in Fig. 4: the incoming and outgoing electrons define the scattering plane; the π^+ and neutron momentum vectors define the hadronic production plane, characterized by polar angles θ_π and θ_n; and ϕ_π defines the angle between the production plane and the electron scattering plane. The differential cross section is then

$$\frac{d^3\sigma}{dE_f d\Omega_e d\Omega} =: \Gamma \frac{d\sigma}{d\Omega}, \tag{3.4}$$

where Γ is the virtual photon flux

$$\Gamma = \frac{\alpha_{\rm em}}{2\pi^2 Q^2} \frac{(W^2 - m_N^2)E_f}{2m_N E_i} \frac{1}{1-\epsilon}. \tag{3.5}$$

Here $\alpha_{\rm em}$ is the fine structure constant and m_N is the nucleon mass; W is the invariant mass of the hadronic final state; $Q^2 = -(e_i - e_f)^2$ is the photon virtuality, where e_i and e_f are the four-momentum vectors of the initial- and final-state electrons, respectively, and E_i and E_f are their respective energies in the laboratory frame. ϵ is the polarization factor of the virtual photon, and Ω_e and Ω are the electron and pion solid angles. The unpolarized differential hadronic cross section has the following ϕ_π dependence:

$$\frac{d\sigma}{d\Omega} = \sigma_{L+T} + \epsilon\sigma_{TT}\cos 2\phi_\pi + \sqrt{2\epsilon(1+\epsilon)}\sigma_{LT}\cos\phi_\pi, \tag{3.6}$$

where the ϕ_π-independent term is defined as $\sigma_{L+T} = \sigma_T + \epsilon\sigma_L$. Distinct from photoproduction, the virtual photon in electroproduction has both transverse and longitudinal polarizations. Resolving the associated kinematic dependences reveals additional information about the production process, e.g., by measuring the ϕ_π dependence of the cross section in Eq. (3.6), one can isolate the terms that describe transverse-transverse and transverse-longitudinal interferences.

C. Electroproduction data at low Q^2

Experiments with CLAS began in 1998. Following commissioning, the CLAS Collaboration took precise data covering a large mass range from pion threshold up to $W = 1.55$ GeV, with $n\pi^+$ and $p\pi^0$ being the final states at two values of Q^2, pursuing a primary goal of studying the low-Q^2 behavior of the proton-Roper transition. Analysis of the data was a complex and time-consuming task.

Resonance electroexcitation amplitudes are extracted from exclusive electroproduction data by employing phenomenological reaction models capable of reproducing the full set of observables measured in the $N\pi$ and $p\pi^+\pi^-$ channels, subject to general reaction theory constraints, such as analyticity and unitarity. When analyzing $n\pi^+$, $p\pi^0$, and $p\eta$ final states, the most frequently used approaches are the unitary isobar model (UIM) (Drechsel *et al.*, 1999; Aznauryan, 2003; Drechsel, Kamalov, and Tiator, 2007) and fixed-t dispersion relations (DRs) (Aznauryan *et al.*, 2005). In both cases, resonances are described by a relativistic Breit-Wigner distribution involving an energy-dependent width. Naturally, it is important to implement a good description of the background contributions. With the UIM approach, these are described explicitly through the inclusion of s- and t-channel meson-exchange processes; whereas in the DR method they are calculated directly from the s-channel resonance terms using dispersion relations. The DR approach is tightly constrained, but the UIM method, involving more fitting parameters, has greater flexibility.

Employing these schemes, the CLAS Collaboration released an analysis of their low-Q^2 data shortly after the beginning of the new millennium (Aznauryan *et al.*, 2005). As illustrated by Fig. 5, both the UIM and DR methods give very similar results, and the CLAS Collaboration used the difference between them as an estimate of systematic uncertainties in the model analysis. In this way they obtained the helicity amplitudes displayed in

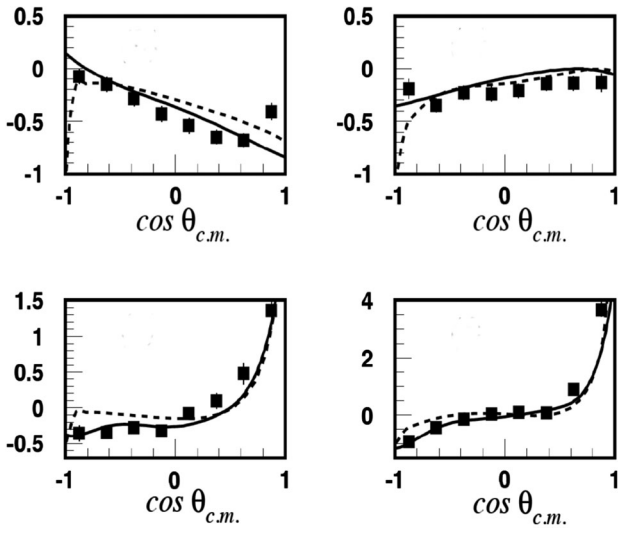

FIG. 5. Cross-section data. (Left panels) $Q^2 = 0.45$ GeV^2 and (right panels) $Q^2 = 0.60$ GeV^2. (Upper panels) $\gamma^* p \to \pi^0 p$ and (lower panels) $\gamma^* p \to \pi^+ n$. The curves are results of global fits to these data using the (solid) UIM and (dashed) DR approaches. [Details provided elsewhere (Aznauryan *et al.*, 2005). The ordinate unit is μb.]

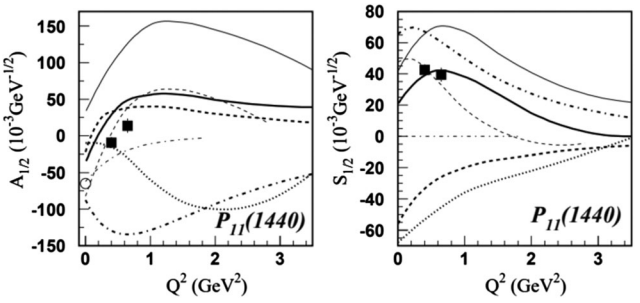

FIG. 6. First results from CLAS on the Roper helicity amplitudes (Aznauryan *et al.*, 2005)—solid squares. All curves are results from various types of CQM: solid bold and solid thin—results obtained using, respectively, relativistic and nonrelativistic versions (Capstick and Keister, 1995); dotted (Warns *et al.*, 1990); dashed (Cano and Gonzalez, 1998); dot-dashed, thin—quark-gluon hybrid model (Li, Burkert, and Li, 1992); and dot-dashed (Tiator *et al.*, 2004). Open circle in left panel—Estimate at photoproduction point from Eidelman *et al.* (2004).

Fig. 6. The results contrast starkly with the pre-2000 data in Fig. 3: now the transverse amplitude shows a clear zero crossing near $Q^2 = 0.5$ GeV^2, the first time this had been seen in any hadron form factor or transition amplitude, and the longitudinal amplitude is large and positive. The power of precise, accurate data on the transition form factors is also evident in Fig. 6: the hybrid (constituent-quark plus gluon) Roper (Li, Burkert, and Li, 1992) and two other constituent-quark models (Warns *et al.*, 1990; Tiator *et al.*, 2004) are eliminated.

The model most favored by the new data is arguably that which describes the Roper as a radial excitation of the nucleon's quark core dressed by a soft meson cloud (Cano and Gonzalez, 1998), where a detailed explanation of this "cloud" is presented in Sec. IV, although the relativistic CQM (Capstick and Keister, 1995) remains viable. Both these calculations predict the zero in the $A_{1/2}$ amplitude, although it is achieved through different mechanisms: the meson cloud is responsible in Cano and Gonzalez (1998) and relativity plays a crucial role in Capstick and Keister (1995). Furthermore, the predictions made by these two models disagree markedly at larger Q^2, i.e., on the domain within which any soft meson-cloud component of a resonance should become invisible to the probe. This is correlated with the differing dynamical origins of the $A_{1/2}$ zero in the two CQMs. It was now clear that higher-Q^2 data are necessary in order to determine the nature of the Roper resonance.

D. Pushing electroproduction experiments to higher Q^2

Using CLAS and the 6 GeV continuous-wave electron beam at JLab, high-statistics data were subsequently collected and analyzed, extending the kinematic range to $W = 2$ GeV and $Q^2 = 4.5$ GeV^2 (Aznauryan *et al.*, 2008, 2009; Aznauryan and Burkert, 2012a; Mokeev *et al.*, 2012, 2016). The new experiments revealed some surprising aspects of the Roper electroproduction amplitudes, overturning conclusions that might have been drawn from the low-Q^2 data alone. For example, as highlighted in Fig. 7, whereas $A_{1/2}$ is small in the low-Q^2 range accessed by the earlier CLAS data, because it is undergoing a sign change at $Q^2 \approx 0.5$ GeV^2, and hence the Roper is not

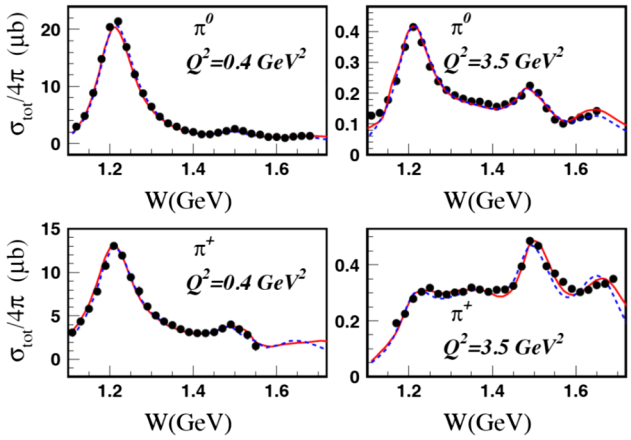

FIG. 7. Lowest moment of the polar-angle dependence in the Legendre expansion of the total cross section σ_{T+L} for the $n\pi^+$ and $p\pi^0$ electroproduction final states, where the solid (red) and dashed (blue) curves represent, respectively, DR and UIM fits (Aznauryan *et al.*, 2009). Evidently, while the $\Delta(1232)$ is the most conspicuous feature at low Q^2 (left panels), the Roper resonance becomes prominent in the $n\pi^+$ final state at large Q^2, generating the broad shoulder centered near $W = 1.35$ GeV (lower right panel). *N.B.* The strong peak at 1.5 GeV owes two other resonances: $N(1520)3/2^-$ and $N(1535)1/2^-$.

directly visible in the total cross section, at high Q^2 this resonance becomes very strong, even dominating over the $\Delta(1232)$ on $Q^2 > 2$ GeV^2 in the $n\pi^+$ final state.

The final data set used in the global fit contained over 120 000 points in $ep \to e'n\pi^+$ and $ep \to e'p\pi^0$, measuring differential cross sections, and polarized beam and polarized target asymmetries, covering the complete range of azimuthal and polar angles, and $W < 1.8$ GeV and $Q^2 < 4.5$ GeV^2. The Roper resonance transverse and longitudinal electroproduction helicity amplitudes obtained from the complete analysis are displayed in Fig. 8. These results confirm those obtained in earlier analyses of much reduced data sets and significantly extend them. Importantly, the evident agreement between independent analyses of single- and double-pion final states boosts confidence in both. [*N.B.* New CLAS data on $\pi^+\pi^- p$ electroproduction (Isupov *et al.*, 2017), with nine onefold differential cross sections covering a final hadron invariant mass range $W \in [1.4, 2.0]$ GeV and $Q^2 \in [2, 5]$ GeV^2, will enable this agreement to be tested further.]

E. Roper resonance: Current experimental status

It is appropriate here to summarize the modern empirical status.

- The Roper $[N(1440)1/2^+]$ is a four-star resonance with pole mass ≈1.37 GeV and width ≈0.18 GeV (Tanabashi *et al.*, 2018).
- Transverse helicity amplitude $A_{1/2}(Q^2)$:
  - — increases rapidly as Q^2 increases from the real photon point to $Q^2 \approx 2$ GeV^2;
  - — changes sign at $Q^2 \approx 0.5$ GeV^2;
  - — exhibits a maximum value at $Q^2 \approx 2$ GeV^2, attaining a magnitude which matches or exceeds that at the real photon point;

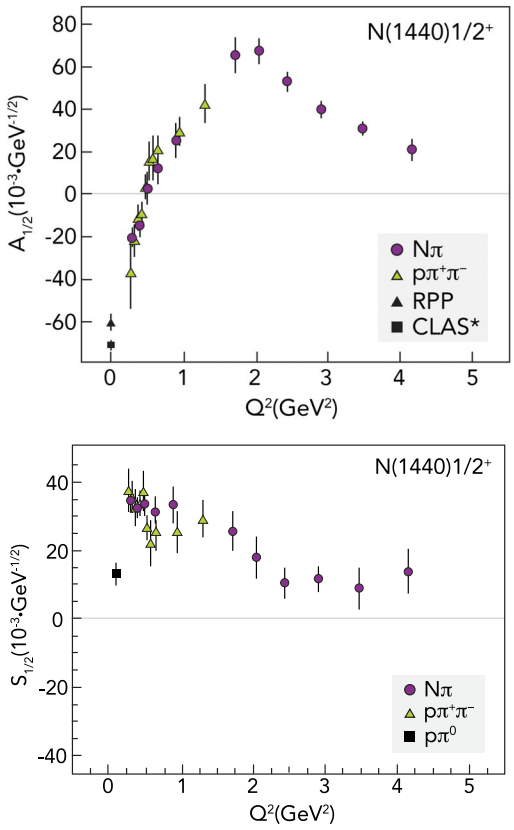

FIG. 8. (Upper panel) Transverse and (lower panel) longitudinal Roper resonance electrocoupling helicity amplitudes. Circles (purple)—analysis of single-pion final states (Aznauryan *et al.*, 2008, 2009); triangles (green)—analysis of $ep \to e'\pi^+\pi^- p'$ (Mokeev *et al.*, 2012, 2016); square (upper panel, black)—CLAS Collaboration result at the photoproduction point (Dugger *et al.*, 2009) and triangle (black)—review of particle properties global average of this value (Tanabashi *et al.*, 2018). Square (lower panel, black)—$Q^2 \simeq 0.1$ GeV^2 $\vec{e}p \to e'\vec{p}\pi^0$ measurement (Štajner *et al.*, 2017).

  - decreases steadily toward zero with increasing Q^2 after reaching its maximum value.
- Longitudinal helicity amplitude $S_{1/2}(Q^2)$:
  - maximal near the real photon point;
  - decreases slowly as Q^2 increases toward 1 GeV^2;
  - decreases more quickly on $Q^2 \gtrsim 1$ GeV^2.
- $N\pi$ and $p\pi^+\pi^-$ final states in electroproduction: The nonresonant contributions to these two final states are markedly dissimilar and hence very different analysis procedures are required to isolate the resonant contributions. Notwithstanding this, the results for the resonant contributions agree on the domain of overlap, i.e., $Q^2 \in [0.25, 1.5]$ GeV^2.

IV. DYNAMICAL COUPLED-CHANNELS CALCULATIONS

As highlighted in Sec. III, the last twenty years have seen an explosion in the amount of available data on the reactions $\gamma^{(*)}N \to \pi N$ and $\gamma^{(*)}N \to \pi\pi N$, which are particularly relevant to discussions of the Roper resonance. As the data accumulated, so grew an appreciation of the need for a sound theoretical analysis which unified all its reliable elements. At the beginning of 2006, this culminated with the establishment of the Excited Baryon Analysis Center (EBAC) at JLab (Lee, 2007, 2013; Kamano and Lee, 2012), whose primary goals are to perform a dynamical coupled-channels (DCC) analysis of the world's data on meson production reactions from the nucleon in order to determine the meson-baryon partial-wave amplitudes, and identify and characterize all nucleon resonances that contribute to these reactions.

In contrast to partial-wave analyses, which are model independent to some extent, but also, therefore, limited in the amount of information they can provide about resonance structure, modern DCC analyses are formulated via a Hamiltonian approach to multichannel reactions (Julia-Diaz *et al.*, 2007; Kamano *et al.*, 2010, 2013; Suzuki *et al.*, 2010; Rönchen *et al.*, 2013). The Hamiltonian expresses model assumptions, e.g., statements about the masses of bare or undressed baryons (in the sense of particle versus quasiparticle) and the dominant meson-baryon reaction channels that transform the bare baryon into the observed quasiparticle. Naturally, such assumptions can be wrong. Equally, the models are flexible; they can be falsified and thereby improved, given the vast amount of existing data, and, used judiciously, they can bridge the gap between data and QCD-connected approaches to the computation of baryon properties.

The EBAC approach (Sato and Lee, 1996; Matsuyama, Sato, and Lee, 2007), for instance, describes meson-baryon (MB) reactions involving the following channels: πN, ηN, and $\pi\pi N$, the last of which has $\pi\Delta$, ρN, and σN resonant components. The excitation of the internal structure of a given initial-state baryon (B) by a meson (M) to produce a bare nucleon resonance $\bar{N}^*$ is implemented by an interaction vertex $\Gamma_{MB\to\bar{N}^*}$. Importantly, the Hamiltonian also contains energy-independent meson-exchange terms $v_{MB,M'B'}$, deduced from widely used meson-exchange models of πN and NN scattering.

In such an approach, the features of a given partial-wave amplitude may be connected with dressing of the bare resonances included in the Hamiltonian ($\bar{N}^*$), in which case the resulting N^* states are considered to be true resonance excitations of the initial-state baryon. On the other hand, they can also be generated by attraction produced by the $v_{MB,M'B'}$ interaction and channel-coupling effects, in which case they are commonly described as "molecular states" so as to differentiate them from true resonance excitations. The need to reliably distinguish between these two different types of systems in the solution of the coupled-channels problem defined by the model Hamiltonian requires that the form and features of $v_{MB,M'B'}$ must be very carefully constrained by, e.g., elastic scattering data, throughout the region of relevance to the resonance production reactions.

Being aware of the challenges associated with understanding the Roper resonance, the EBAC Collaboration made a determined effort to produce a sound description of the spectrum of baryon resonances with masses below 2 GeV using their DCC model. Refining this tool by developing a description of 22 348 independent data points, representing the complete array of partial waves, they arrived at some striking conclusions (Julia-Diaz *et al.*, 2007; Kamano *et al.*, 2010; Suzuki *et al.*, 2010), illustrated in Fig. 9.

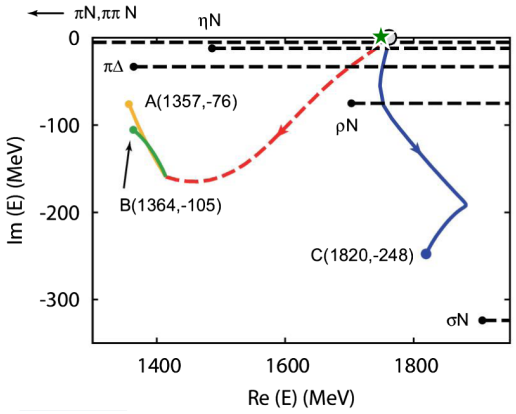

FIG. 9. Open circle (black): mass of the bare Roper state determined in the EBAC DCC analysis of πN scattering (Julia-Diaz *et al.*, 2007; Kamano *et al.*, 2010; Suzuki *et al.*, 2010). This bare Roper state, with full spectral weight at mass 1.763 GeV, splits and evolves following the inclusion of meson-baryon final-state interactions, with the trajectories in this complex-energy plane depicting the motion of the three, distinct daughter poles as the magnitude of those interactions is increased from zero to their full strength. The horizontal dashed lines (black) mark the branch cuts associated with all thresholds relevant to the solution of the DCC scattering problem in this channel. Solid star (green): mass of the dressed-quark core of the proton's first radial excitation predicted by a three valence-quark Faddeev equation (Segovia *et al.*, 2015).

- From a bare state with mass 1.763 GeV, three distinct features appear in the P_{11} partial wave, as described by Fig. 9. (We will subsequently return to the interpretation of the bare state.)
- Of the three spectral features that emerge in this channel, two are associated with the Roper resonance. [This two-pole character of the Roper is common to many analyses of the scattering data, including one involving Roper himself (Arndt, Ford, and Roper, 1985) and more recent analyses of πN scattering data (Cutkosky and Wang, 1990; Arndt *et al.*, 2006; Döring *et al.*, 2009).]
- The third pole is located farther from the origin (position C in Fig. 9) and might plausibly be associated with the $N(1710)1/2^+$ state listed by the Particle Data Group (Tanabashi *et al.*, 2018).

[N.B. (i) The same EBAC DCC analysis identified a bare state with mass 1.800 GeV as the origin of the $N(1535)1/2^-$ and a bare state with mass 1.391 GeV associated with the $\Delta(1232)3/2^+$ (Julia-Diaz *et al.*, 2007). (ii) Despite the seemingly large amount of independent data used, the set is incomplete, e.g., polarized target information is lacking in some regions. It is conceivable therefore that such bare masses might shift somewhat with the acquisition of additional data. This cannot affect the electroproduction form factors, however, because they are independent of these pieces of the DCC models.]

The trajectories in Fig. 9 emphasize that the coupling between channels, required to simultaneously describe all partial waves, has an extraordinary effect with, e.g., numerous spectral features in the P_{11} channel evolving from a single bare state, expressed as a pole on the real axis, through its coupling to the πN, ηN, and $\pi\pi N$ reaction channels. Hence, no analysis of one partial wave in isolation can reasonably be claimed to provide an understanding of such a complex array of emergent features.

V. RELATIVISTIC QUANTUM FIELD THEORY

A. Lattice-regularized QCD

An introduction to the numerical simulation of lattice-regularized QCD (lQCD) is provided elsewhere (Gattringer and Lang, 2010), so here we simply note that this method is a nonperturbative approach to solving QCD in which the gluon and quark fields are quantized on a discrete lattice of finite extent, whose intersections each represent a point in spacetime (Wilson, 1974).

The lQCD approach has provided a spectrum of light ground-state hadrons that agree with experiment (Durr *et al.*, 2008), but numerous hurdles are encountered in attempting to compute properties of resonance states in this way (Liu, 2017; Briceno, Dudek, and Young, 2018). In connection with the Roper, which in reality couples strongly to many final-state interaction (FSI) channels, as indicated in Fig. 9, these include the following: the challenges of computing with a realistic pion mass and developing both a fully representative collection of interpolating fields and a valid strategy for handling all contributing final-state interaction channels, which incorporate the issue of ensuring that the nucleon's lowest excitations are properly isolated from all higher excitations; and the problem of veraciously expressing chiral symmetry and the pattern by which it is broken in both the fermion action and the algorithm used in performing the simulation.

Much needs to be learned and implemented before these problems are overcome, so the current status of lQCD results for the Roper is unsettled. This is illustrated in Fig. 10, which provides a snapshot of recent results for the masses of the

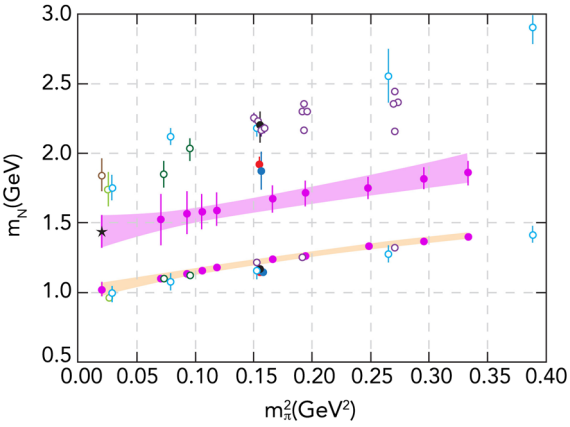

FIG. 10. Illustrative collection of lQCD results for the mass of the nucleon (lower band) and its lightest positive-parity excitation as a function of m_π^2, where m_π is the pion mass used in the simulation. The results depicted were obtained with different lattice formulations and varying methods for identifying the excited state, as described in the source material (Edwards *et al.*, 2011; Alexandrou *et al.*, 2015; Liu *et al.*, 2014; Mahbub *et al.*, 2012; Engel *et al.*, 2013; Liu, 2017).

nucleon and its lowest-mass positive-parity excitation. In this image, almost all formulations of the lQCD problem produce values that extrapolate (as m_π^2 is taken toward its empirical value) to a Roper mass of roughly 1.8 GeV, i.e., to a mass that is 0.4 GeV above the real part of the empirical value, viz. 1.4 GeV. One band, though, appears to extrapolate to somewhere near this empirical value. Contrary to the other formulations, the fermion action in that case (Liu *et al.*, 2014) possesses good chiral symmetry properties. Its proponents conjecture (Liu, 2017) that this feature enables the simulation to better incorporate aspects of the extensive dynamical channel couplings which are known to be important in explaining and understanding the spectral features of πN scattering in the P_{11} channel (Julia-Diaz *et al.*, 2007; Kamano *et al.*, 2010; Suzuki *et al.*, 2010). This speculation remains unproven, however.

As emphasized heretofore, computing a value (even correct) for the Roper mass is insufficient to validate a formulation of the Roper resonance problem and its solution. An additional and far more stringent test is an explanation of the pointwise behavior of the transition form factors measured in electroproduction, Eq. (3.1). The first such lQCD calculations, which used the quenched truncation of the theory, are described by Lin *et al.* (2008). More recently, results were obtained with two light quarks and one strange quark ($N_f = 2 + 1$) (Lin and Cohen, 2012). They are depicted in Fig. 11. These simulations identified the Roper resonance with the first positive-parity excitation of the nucleon, whose computed mass is roughly 1.8 GeV, and focused on the low-Q^2 domain. Significantly, compared with the quenched results, the inclusion of $N_f = 2 + 1$ dynamical fermions produces a sign change in F_2^*, located in the same neighborhood as that seen in experimental data. This difference between quenched and dynamical simulations once again suggests that meson-baryon (MB) FSIs are a critical part of the long-wavelength structure of the Roper.

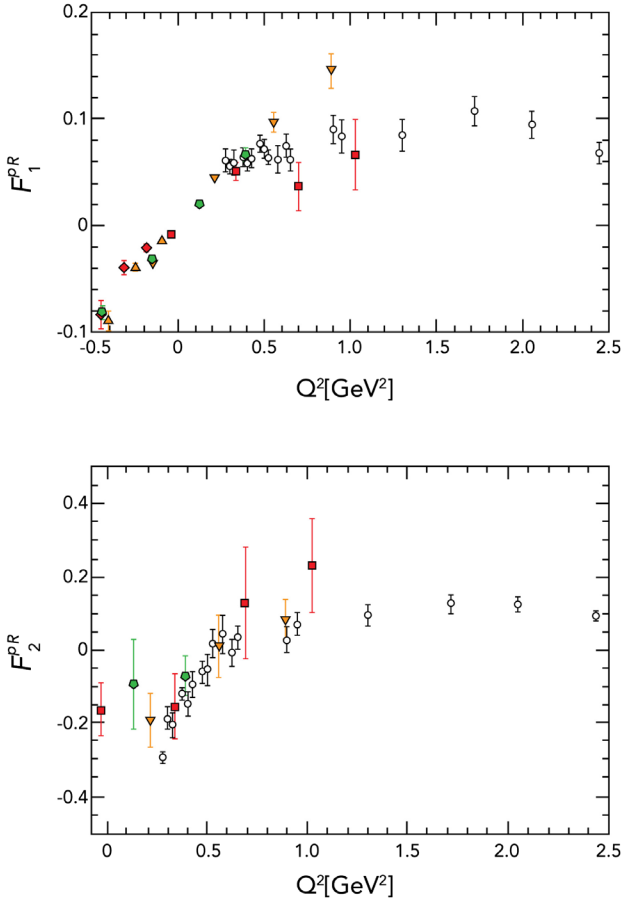

FIG. 11. Existing results for the (upper panel) Dirac and (lower panel) Pauli proton-Roper transition form factors computed using the methods of lQCD (Lin and Cohen, 2012) on anisotropic lattices with pion masses (in GeV): 0.39 (red squares), 0.45 (orange triangles), and 0.875 (green circles); and associated spatial lengths of 3, 2.5, and 2.5 fm. Open circles are empirical results from the CLAS Collaboration (Aznauryan *et al.*, 2009; Dugger *et al.*, 2009; Mokeev *et al.*, 2012, 2016).

B. Insight from continuum analyses

An approach to developing a solution of QCD in the continuum is provided by the Dyson-Schwinger equations (DSEs) (Roberts and Williams, 1994; Chang, Roberts, and Tandy, 2011; Bashir *et al.*, 2012; Eichmann *et al.*, 2016; Horn and Roberts, 2016; Roberts, 2016), which define a symmetry-preserving (and hence Poincaré covariant) framework with a traceable connection to the QCD Lagrangian. The challenge in this approach is the need to employ a truncation in order to define a tractable bound-state problem. Much has been learned in the past twenty years, and one may now separate DSE predictions into three classes: class A—model-independent statements about QCD, class B—illustrations of such statements using well-constrained model elements and possessing a traceable connection to QCD, and class C—QCD-based analyses whose elements have not been computed using a truncation that preserves a systematically improvable connection with QCD.

The treatment of a baryon as a continuum three-valence-body bound-state problem became possible following the formulation of a Poincaré-covariant Faddeev equation (Burden, Cahill, and Praschifka, 1989; Cahill, 1989; Cahill, Roberts, and Praschifka, 1989; Efimov, Ivanov, and Lyubovitskij, 1990; Reinhardt, 1990), which is depicted in Fig. 12. The ensuing years have seen studies increase in breadth and sophistication. In order to understand the current status, it is apt to begin by elucidating the nature of the

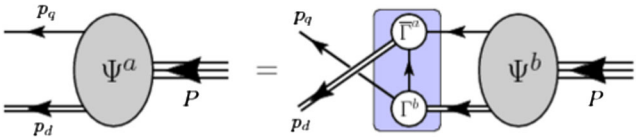

FIG. 12. Poincaré covariant Faddeev equation: a homogeneous linear integral equation for the matrix-valued function Ψ, being the Faddeev amplitude for a baryon of total momentum $P = p_q + p_d$, which expresses the relative momentum correlation between the dressed quarks and diquarks within the baryon. The shaded rectangle demarcates the kernel of the Faddeev equation: single line, dressed-quark propagator; Γ, diquark correlation amplitude; and double line, diquark propagator. Further details are provided in Sec. V.B.

individual "bodies" whose interactions are described by that Faddeev equation.

It is worth opening with an observation, viz. although it is commonly thought that the Higgs boson is the origin of mass, that is incorrect: it gives mass only to some very simple particles, accounting for just 1%–2% of the weight of more complex entities, such as atoms and molecules. Instead, the vast bulk of visible mass is generated dynamically by interactions in QCD (Wilczek, 2012). This remark is readily substantiated by noting that the mass scale for the spectrum of strongly interacting matter is characterized by the proton's mass $m_N \approx 1$ GeV $\approx 2000 m_e$, where m_e is the electron mass. However, the only apparent scale in chromodynamics is the current-quark mass. This is the quantity generated by the Higgs boson; but, empirically, the current mass is more than 2 orders of magnitude smaller (Tanabashi *et al.*, 2018). No amount of "staring" at the Lagrangian for QCD can reveal the source of that enormous amount of "missing mass." Yet, it must be there and exposing the character of the Roper resonance is critical to understanding the nature of strong mass generation within the standard model.

One of the keys to resolving this conundrum is the phenomenon of DCSB (Nambu, 2011), which can be exposed in QCD by solving the quark gap equation, i.e., the DSE for the dressed-quark Schwinger function (propagator) (Roberts and Williams, 1994):

$$S(p) = Z(p^2)/[i\gamma \cdot p + M(p^2)], \tag{5.1}$$

where $M(p^2)$ is the dressed-quark mass function. Whether or not DCSB emerges in the standard model is decided by the structure of the gap equation's kernel. Hence the basic question is just what form does that kernel take? Owing to asymptotic freedom, the answer is known on the perturbative domain $\mathcal{A} = \{(p,q)|k^2 = (p-q)^2 \simeq p^2 \simeq q^2 \gtrsim 2\ \mathrm{GeV}^2\}$. The question thus actually relates only to the infrared domain, which is a complement of $\mathcal{A}$ and so resides in sQCD.

The gap equation's kernel is built from the QCD running coupling, dressed-gluon propagator and dressed-gluon-quark vertex. The past two decades have revealed much about these quantities, and the current state of understanding can be traced from an array of sources (Boucaud *et al.*, 2012; Binosi *et al.*, 2015; Aguilar, Binosi, and Papavassiliou, 2016; Binosi, Chang *et al.*, 2017; Binosi, Mezrag *et al.*, 2017). Of particular interest is the feature that the gluon propagator saturates at infrared momenta, i.e.,

$$\Delta(k^2 \simeq 0) = 1/m_g^2, \tag{5.2}$$

which entails that the long-range propagation characteristics of gluons are dramatically affected by their self-interactions. Importantly, one may associate a renormalization-group-invariant gluon mass scale with this effect: $m_0 \approx 0.5$ GeV $\approx m_N/2$ (Binosi *et al.*, 2015; Cyrol *et al.*, 2016; Binosi, Mezrag *et al.*, 2017), and summarize a large body of work, which began roughly thirty-five years ago (Cornwall, 1982), by stating that gluons, although acting as massless degrees of freedom on the perturbative domain, actually possess a running mass, whose value at infrared momenta is characterized by m_0.

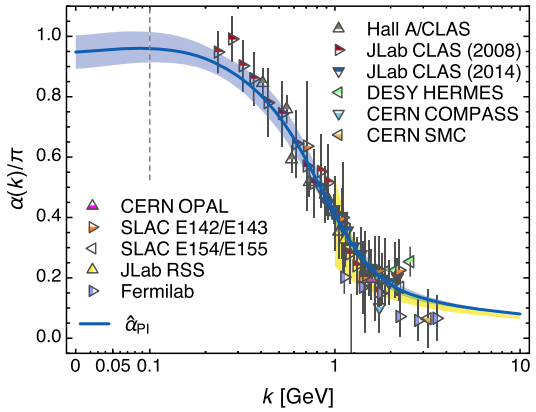

FIG. 13. Solid (blue) curve: process-independent running coupling $\hat{\alpha}_{\rm PI}(k^2)$ (Binosi, Mezrag *et al.*, 2017). The shaded (blue) band bracketing this curve combines a 95% confidence-level window based on existing lQCD results for the gluon two-point function with an error of 10% in the continuum analysis of relevant ghost-gluon dynamics. World data on the process-dependent effective coupling α_{g_1}, defined via the Bjorken sum rule (Anthony *et al.*, 1993, 1996, 1999a, 1999b, 2000, 2003; Abe *et al.*, 1995a, 1995b, 1995c, 1996, 1997a, 1997b, 1997c, 1998; Ackerstaff *et al.*, 1997, 1998; Airapetian *et al.*, 1998, 2003, 2007; Kim *et al.*, 1998; Alexakhin *et al.*, 2007; Deur *et al.*, 2007, 2008, 2014; Alekseev *et al.*, 2010; Adolph *et al.*, 2016). The shaded (yellow) band on $k > 1$ GeV represents α_{g_1} obtained from the Bjorken sum by using QCD evolution (Gribov and Lipatov, 1972; Altarelli and Parisi, 1977; Dokshitzer, 1977) to extrapolate high-k^2 data into the depicted region (Deur *et al.*, 2007, 2008).

The mathematical tools that have enabled theory to arrive at this conclusion (Abbott, 1981, 1982; Cornwall, 1982; Cornwall and Papavassiliou, 1989; Pilaftsis, 1997; Binosi and Papavassiliou, 2002, 2004, 2009) can also be used to compute a *process-independent* running coupling $\hat{\alpha}_{\rm PI}(k^2)$ (Binosi, Mezrag *et al.*, 2017). Depicted as the solid (blue) curve in Fig. 13, this is a new type of effective charge, which is an analog of the Gell-Mann–Low effective coupling in QED (Gell-Mann and Low, 1954), because it is completely determined by the gauge-boson propagator. The result in Fig. 13 is a parameter-free class-A prediction, capitalizing on analyses of QCD's gauge sector undertaken using both continuum methods and numerical simulations of lQCD.

The data in Fig. 13 represent empirical information on α_{g_1}, a process-dependent effective charge (Grunberg, 1984) determined from the Bjorken sum rule, one of the most basic constraints on our knowledge of nucleon spin structure. Sound theoretical reasons underpin the almost precise agreement between $\hat{\alpha}_{\rm PI}$ and α_{g_1} (Binosi, Mezrag *et al.*, 2017), so that the Bjorken sum may be seen as a near direct means by which to gain empirical insight into QCD's Gell-Mann–Low effective charge. Given the behavior of the prediction in Fig. 13, it is evident that the coupling is everywhere finite in QCD, i.e., there is no Landau pole, and this theory possesses an infrared-stable fixed point. Evidently, QCD is infrared finite owing to the dynamical generation of a gluon mass scale.

As a unique process-independent effective charge, $\hat{\alpha}_{\rm PI}$ appears in every one of QCD's dynamical equations of motion, setting the interaction strength in all cases, including the dressed-quark gap equation. It therefore plays a crucial role in determining the fate of chiral symmetry.

The remaining element in the gap equation is the dressed gluon-quark vertex Γ_ν. If this vertex were only weakly modified from its tree-level form γ_ν then, with $\hat{\alpha}_{\rm PI}$ in Fig. 13, chiral symmetry would be preserved in nature (Binosi, Chang *et al.*, 2017). It is not, and after nearly forty years of studying Γ_ν, with numerous contributions that may be traced from an analysis of Abelian theories (Ball and Chiu, 1980), continuum and lattice efforts have revealed just how the vertex is dressed so that DCSB is unavoidable. Namely, the smooth, infrared-finite coupling depicted in Fig. 13 is strong enough to force nonzero values for those terms in Γ_ν which usually vanish in the chiral limit. This seeds a powerful positive feedback chain so that chiral symmetry is not only broken, but there is a sense in which it is very difficult to keep the growth of the dressed-quark mass function $M(p^2)$, within physically reasonable bounds (Binosi, Chang *et al.*, 2017). Consequently, the gap equation's solution, Eq. (5.1), describes a dressed quark with a dynamically generated running mass that is large in the infrared $M(p^2 \simeq 0) \approx 0.3$ GeV, as illustrated in Fig. 14.

It is dressed quarks characterized by the mass function in Fig. 14 that are the basic elements in the Faddeev equation depicted in Fig. 12. Solving this equation in all allowed channels, one obtains the baryon spectrum and simultaneously the amplitudes necessary to compute transitions between ground and excited states. As highlighted elsewhere (Cloët, Roberts, and Thomas, 2013; Binosi, Chang *et al.*, 2017), this means that since quarks carry electric charge, experiments involving electron scattering from hadrons can probe the momentum dependence of this mass function and also its collateral influences. Measurements at the upgraded JLab facility will explore a region that is indicated approximately by the shading in Fig. 14, i.e., the domain of transition from strong to perturbative QCD.

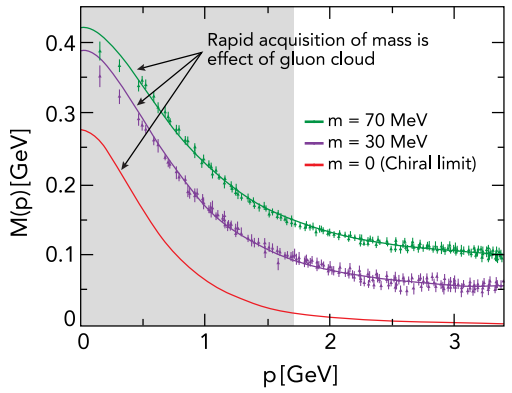

FIG. 14. Dressed-quark mass function $M(p)$ in Eq. (5.1). Solid curves—gap equation results (Bhagwat *et al.*, 2003; Bhagwat and Tandy, 2006), "data"—numerical simulations of lQCD (Bowman *et al.*, 2005). The current quark of perturbative QCD evolves into a constituent quark as its momentum decreases. The constituent mass arises from a cloud of low-momentum gluons attaching themselves to the current quark. This is DCSB, the nonperturbative effect that generates a quark *mass from nothing*; namely, it occurs even in the chiral limit. Notably, the size of $M(0)$ is a measure of the magnitude of the QCD scale anomaly in $n = 1$ point Schwinger functions (Roberts, 2017), and experiments on $Q^2 \in [0, 12]$ GeV^2 at the upgraded JLab facility are sensitive to the momentum dependence of $M(p)$ within a domain that is here indicated approximately by the shaded region.

Contemporary theory indicates that DCSB is responsible for more than 98% of the visible mass in the Universe (Brodsky *et al.*, 2015). Simultaneously, it ensures the existence of nearly massless pseudo–Nambu-Goldstone modes (pions), each constituted from a valence quark and antiquark whose individual Lagrangian current-quark masses are $< 1\%$ of the proton mass (Maris, Roberts, and Tandy, 1998).

Another important consequence of DCSB is less well known. Namely, any interaction capable of creating pseudo–Nambu-Goldstone modes as bound states of a light dressed quark and antiquark, and reproducing the measured values of their leptonic decay constants, must also generate strong color-antitriplet correlations between any two dressed quarks contained within a nucleon. Although a rigorous proof within QCD cannot be claimed, this assertion is based upon an accumulated body of evidence, gathered in two decades of studying bound-state problems in hadron physics (Segovia, Roberts, and Schmidt, 2015). No realistic counterexamples are known, and the existence of such diquark correlations is also supported by lQCD (Alexandrou, de Forcrand, and Lucini, 2006; Babich *et al.*, 2007).

The properties of such diquark correlations have been charted. As color-carrying correlations, diquarks are confined (Bender, Roberts, and von Smekal, 1996; Bender *et al.*, 2002; Bhagwat *et al.*, 2004). Additionally, owing to properties of charge conjugation, a diquark with spin parity J^P may be viewed as a partner to the analogous J^{-P} meson (Cahill, Roberts, and Praschifka, 1987). It follows that the strongest diquark correlations are scalar isospin zero $[ud]_{0^+}$; and pseudovector, isospin one $\{uu\}_{1^+}$, $\{ud\}_{1^+}$, and $\{dd\}_{1^+}$. Moreover, while no pole mass exists, the following mass scales, which express the strength and range of the correlation, may be associated with these diquarks (Cahill, Roberts, and Praschifka, 1987; Maris, 2002; Alexandrou, de Forcrand, and Lucini, 2006; Babich *et al.*, 2007; Eichmann, Fischer, and Sanchis-Alepuz, 2016; Lu *et al.*, 2017; Chen *et al.*, 2018) (in GeV):

$$m_{[ud]_{0^+}} \approx 0.7\text{–}0.8, \qquad m_{\{uu\}_{1^+}} \approx 0.9\text{–}1.1, \tag{5.3}$$

where $m_{\{dd\}_{1^+}} = m_{\{ud\}_{1^+}} = m_{\{uu\}_{1^+}}$ in the isospin symmetric limit. The nucleon contains both scalar-isoscalar and pseudovector-isovector correlations: neither can be ignored and their presence has many observable consequences (Roberts, Holt, and Schmidt, 2013; Segovia, Chen *et al.*, 2014).

Realistic diquark correlations are also soft and interacting. All carry charge, scatter electrons, and possess an electromagnetic size which is similar to that of the analogous mesonic system, e.g. (Maris, 2004; Eichmann *et al.*, 2009; Roberts *et al.*, 2011): $r_{[ud]_{0^+}} \gtrsim r_\pi$, $r_{\{uu\}_{1^+}} \gtrsim r_\rho$, with

$r_{\{uu\}_{1^+}} > r_{[ud]_{0^+}}$. As in the meson sector, these scales are set by that associated with DCSB.

Importantly, these dynamical diquark correlations are vastly different from the static, pointlike "diquarks" which featured in early attempts (Lichtenberg and Tassie, 1967; Lichtenberg, Tassie, and Keleman, 1968) to understand the baryon spectrum and explain the so-called missing resonance problem, viz. the fact that quark models predict many more baryon states than were observed in the previous millennium (Burkert and Lee, 2004). As stated, modern diquarks are soft. They also enforce distinct interaction patterns for the singly and doubly represented valence quarks within the proton (Roberts, Holt, and Schmidt, 2013; Segovia, Cloët *et al.*, 2014; Roberts, 2016; Segovia and Roberts, 2016). Nevertheless, the number of states in the spectrum of baryons obtained from the Faddeev equation (Eichmann, Fischer, and Sanchis-Alepuz, 2016; Lu *et al.*, 2017; Chen *et al.*, 2018) is similar to that found in the three-constituent quark model, just as it is in lQCD spectrum calculations (Edwards *et al.*, 2011). [Notably, modern data and recent analyses have already reduced the number of missing resonances (Ripani *et al.*, 2003; Burkert, 2012; Crede and Roberts, 2013; Kamano *et al.*, 2013; Mokeev *et al.*, 2016; Anisovich *et al.*, 2017).]

The existence of these tight correlations between two dressed quarks is the key to transforming the three valence-quark scattering problem into the simpler Faddeev equation problem illustrated in Fig. 12, without loss of dynamical information (Eichmann *et al.*, 2010; Segovia, Roberts, and Schmidt, 2015). The active kernel here describes binding within the baryon through diquark breakup and reformation, which is mediated by exchange of a dressed quark, and such a baryon is a compound system whose properties and interactions are largely determined by the quark + diquark structure evident in Fig. 12.

This approach to the baryon bound-state problem has been used to calculate a wide range of nucleon-related observables (Wilson *et al.*, 2012; Chang, Roberts, and Schmidt, 2013; Roberts, Holt, and Schmidt, 2013; Segovia, Cloët *et al.*, 2014; Roberts, 2015; Xu *et al.*, 2015; Eichmann *et al.*, 2016; Segovia and Roberts, 2016), in particular, in the computation of the mass and structure of the nucleon and its first radial excitation (Segovia *et al.*, 2015). This class-C analysis begins by solving the Faddeev equation to obtain the masses and Poincaré-covariant wave functions for these systems, taking each element of the equation to be as specified by Segovia, Cloët *et al.* (2014), which provides a successful description of the properties of the nucleon and Δ baryon. With those inputs, the masses are (in GeV)

$$\text{nucleon}\,(N) = 1.18, \quad \text{nucleon excited}\,(R) = 1.73. \tag{5.4}$$

These masses correspond to the locations of the two lowest-magnitude $J^P = 1/2^+$ poles in the three dressed-quark scattering problem. The associated residues are the Faddeev wave functions, which depend upon $(\ell^2, \ell \cdot P)$, where ℓ is the quark-diquark relative momentum and P is the baryon's total momentum. Figure 15 depicts the zeroth Chebyshev moment of all S-wave components in that wave function, i.e., projections of the form

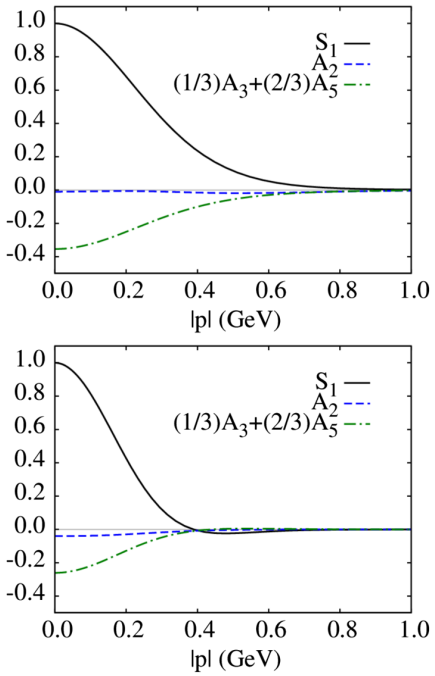

FIG. 15. (Upper panel) Zeroth Chebyshev moment of all S-wave components in the nucleon's Faddeev wave function, which is obtained from Ψ in Fig. 12, by reattaching the dressed quark and diquark legs. (Lower panel) Kindred functions for the first $J^P = 1/2^+$ excited state. S_1 is associated with the baryon's scalar diquark; the other two curves are associated with the axial-vector diquark, and here the normalization is chosen such that $S_1(0) = 1$.

$$\mathcal{W}(\ell^2; P^2) = \frac{2}{\pi}\int_{-1}^{1} du \sqrt{1-u^2}\,\mathcal{W}(\ell^2, u; P^2), \tag{5.5}$$

where $u = \ell \cdot P/\sqrt{\ell^2 P^2}$. The appearance of a single zero in S-wave components of the Faddeev wave function associated with the first excited state in the three dressed-quark scattering problem indicates that this state is a radial excitation (Höll, Krassnigg, and Roberts, 2004; Qin *et al.*, 2012; Rojas, El-Bennich, and de Melo, 2014). Notably, one may associate a four-vector length scale of $1/(0.4\ \text{GeV}) \approx 0.5$ fm with the location of this zero. [Similar conclusions have been drawn using lQCD (Roberts, Kamleh, and Leinweber, 2013).]

Consider now the masses in Eq. (5.4). As discussed in connection with Fig. 9, the empirical values of the pole locations for the first two states in the nucleon channel are 0.939 GeV for the nucleon and two poles for the Roper $1.357 - i0.076$ and $1.364 - i0.105$ GeV. At first glance, these values appear unrelated to those in Eq. (5.4). However, deeper consideration reveals (Eichmann *et al.*, 2008, 2009) that the kernel in Fig. 12 omits all those resonant contributions which may be associated with the MB FSIs (meson-baryon final-state interactions) that are resummed in dynamical coupled channels models (Julia-Diaz *et al.*, 2007; Kamano *et al.*, 2010; Suzuki *et al.*, 2010; Kamano *et al.*, 2013; Rönchen *et al.*, 2013; Döring, 2014) in order to transform a bare baryon into the observed state. The Faddeev equation analyzed to produce the results in Eq. (5.4) should therefore be understood as

producing the *dressed-quark core* of the bound state, not the completely dressed and hence observable object.

Clothing the nucleon's dressed-quark core by including resonant contributions to the kernel produces a physical nucleon whose mass is ≈0.2 GeV lower than that of the core (Ishii, 1998; Hecht *et al.*, 2002; Chang *et al.*, 2009; Sanchis-Alepuz, Fischer, and Kubrak, 2014). Similarly, clothing the Δ baryon's core lowers its mass by ≈0.16 GeV (Julia-Diaz *et al.*, 2007). It is therefore no coincidence that (in GeV) $1.18 - 0.2 = 0.98 \approx 0.94$, i.e., the nucleon mass in Eq. (5.4) is 0.2 GeV greater than the empirical value. A successful body of work on the baryon spectrum (Lu *et al.*, 2017) and nucleon and Δ elastic and transition form factors (Segovia, Cloët *et al.*, 2014; Roberts, 2015; Segovia and Roberts, 2016) has been built upon this assessment of the impact of omitting resonant contributions and the magnitude of their effects. Hence, a comparison between the empirical value of the Roper resonance pole position and the computed dressed-quark-core mass of the nucleon's radial excitation is not the critical test. Instead, it is that between the masses of the quark core and the value determined for the meson-undressed bare Roper. This comparison is presented in Table I. Evidently, as already displayed in Fig. 9, the DCC bare-Roper mass agrees with the quark-core results obtained using both a QCD-kindred interaction (Segovia *et al.*, 2015) and refined treatments of a vector ⊗ vector contact interaction (Wilson *et al.*, 2012; Lu *et al.*, 2017). (It is also commensurate with the value obtained in simulations of lQCD whose formulation and/or parameters suppress MB FSIs, Fig. 10.) This is notable because all these calculations are independent, with just one common feature, viz. an appreciation that observed hadrons should realistically be built from a dressed-quark core plus a meson cloud.

The agreement in Table I is suggestive but not conclusive because the same mass is obtained from the Faddeev equation using vastly different basic interactions. Plainly, the mass alone does not serve as a fine discriminator between theoretical pictures of the nucleon's first radial excitation and its possible identification with the Roper. Critical additional tests are imposed by requiring that the theoretical picture combine a prediction of the Roper's mass with detailed descriptions of its structure and how that structure is revealed in the momentum dependence of the proton-Roper transition form factors. It must also combine all this with a similarly complete picture of the proton, from which the Roper is produced. As detailed in Sec. III, precise empirical information is now available on the proton-Roper transition form factors, reaching momentum transfers $Q^2 \approx 4.5\ \mathrm{GeV}^2$. At such scales, these form factors probe a domain whereupon hard dressed-quark degrees of freedom could be expected to determine their behavior.

TABLE I. Quark-core mass of the Roper resonance determined using different approaches. Row 1 is the value obtained using EBAC's DCC approach, and the remaining three rows are separate DSE computations. (Masses are listed in GeV.)

Approach	Roper quark-core mass
DCC (Suzuki *et al.*, 2010)	1.76
DSE (1) (Segovia *et al.*, 2015)	1.73
DSE (2) (Wilson *et al.*, 2012)	1.72
DSE (3) (Lu *et al.*, 2017)	1.82

Finally, to increase the level of confidence, one should impose an additional test, requiring that the theoretical picture also explains all related properties of the Δ^+ baryon, which is typically viewed as the proton's spin-flip excitation.

With wave functions for the participating states in hand, computation of the transition form factors in Eq. (3.1) is a straightforward numerical exercise. In any computation of such form factors, one must first calculate the analogous elastic form factors for the states involved because the associated values of $F_1(Q^2 = 0)$ fix the normalization of the transition. These normalizations also reveal the diquark content of the bound states (Roberts, Holt, and Schmidt, 2013; Segovia, Cloët *et al.*, 2014; Segovia *et al.*, 2015) and predict that the relative strength of scalar and axial-vector diquark correlations in the nucleon and its radial excitation is the same with $P_{J=0\times 0} = 62\%$. However, the result is sensitive to the quark-quark interaction so this is a prediction that is tested by experiment. Charge radii may also be computed from the elastic form factors, with the result (Segovia *et al.*, 2015) $r^{\Psi}_{R^+}/r^{\Psi}_{p} = 1.8$, i.e., a quark-core radius for the radial excitation that is 80% larger than that of the ground state. In contrast, nonrelativistic harmonic oscillator wave functions yield a value of 1.5 for this ratio. The difference highlights the impact of orbital angular momentum and spin-orbit repulsion, which is introduced by relativity into the Poincaré-covariant Faddeev wave functions for the nucleon and its radial excitation and increases the size of both systems. The ratio of magnetic radii is 1.6.

The form factors predicted by Segovia *et al.* (2015) to describe the transition between the proton and its first radial excitation are depicted in Fig. 16. The Dirac transition form factor F_1^* vanishes at $x = Q^2/m_N^2 = 0$ owing to orthogonality between the proton and its radial excitation. The calculations (gray bands) agree quantitatively in magnitude and qualitatively in trend with the data on $x \gtrsim 2$. Crucially, nothing was tuned to achieve these results. Instead, the outcome owes fundamentally to the QCD-derived momentum dependence of the propagators and vertices employed in the bound state and scattering problems. This point is further highlighted by the contact-interaction result (dot-dashed red): with momentum-independent masses and vertices, the prediction disagrees both quantitatively and qualitatively with the data. Experiment is evidently a sensitive tool with which to chart the nature of the quark-quark interaction and hence discriminate between competing theoretical hypotheses, and it is plainly favoring an interaction that produces a momentum-dependent quark mass of the form in Fig. 14, which characterizes QCD.

The mismatch on $x \lesssim 2$ between data and the prediction in Segovia *et al.* (2015) is also revealing. As emphasized, that calculation yields only those form factor contributions generated by a rigorously defined dressed-quark core whereas meson-cloud contributions are expected to be important on $x \lesssim 2$. Thus, the difference between the prediction and data may plausibly be attributed to MB FSIs. One can estimate the size of this correction by recognizing that the dressed-quark-core component of the baryon Faddeev amplitudes should be renormalized by inclusion of meson-baryon "Fock-space" components, and an array of analyses indicates that one may conservatively represent this effect via a 20% reduction in strength for the quark-core component of the Faddeev amplitude (Bijker and Santopinto, 2009; Cloët and Roberts,

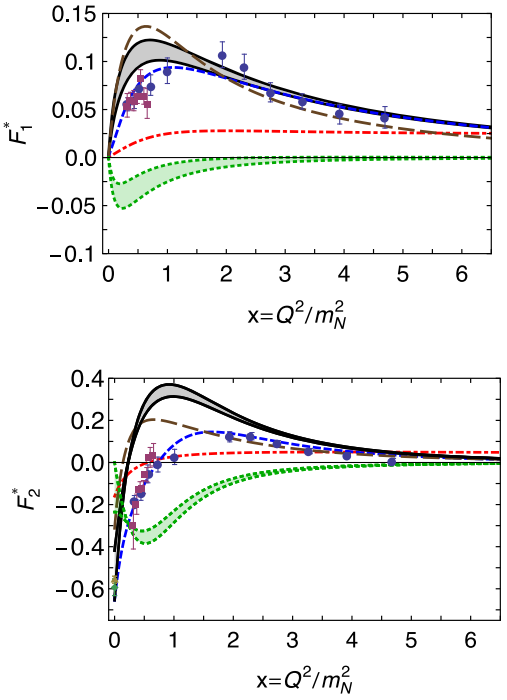

FIG. 16. (Upper panel) F_1^* as a function of $x = Q^2/m_N^2$. Gray band within black curves—dressed-quark-core contribution with up to 20% Faddeev amplitude renormalization from MB FSIs, implemented according to Eq. (5.6a). The transition form factor curve with smallest magnitude at $x = 1$ has the maximum renormalization. Green band within dotted green curves—inferred MB FSI contribution. The band demarcates the range of uncertainty arising from 0% to 20% renormalization of the dressed-quark core. Dashed blue curve—least-squares fit to the data on $x \in (0, 5)$. Dot-dashed red curve—contact-interaction result (Wilson *et al.*, 2012). Long-dashed brown curve—light-front (LF) CQM result reconstructed from the helicity amplitudes in Aznauryan and Burkert (2016) using Eqs. (3.2). (Lower panel) $F_2^*(x)$ with the same legend. Data: circles (blue) (Aznauryan *et al.*, 2009), triangle (gold) (Dugger *et al.*, 2009), squares (purple) (Mokeev *et al.*, 2012, 2016), and star (green) (Tanabashi *et al.*, 2018).

2008; Eichmann *et al.*, 2009; Aznauryan and Burkert, 2016). Naturally, since wave functions in quantum field theory evolve with resolving scale (Lepage and Brodsky, 1979, 1980; Efremov and Radyushkin, 1980; Raya *et al.*, 2016; Gao *et al.*, 2017), the magnitude of this effect is not fixed. Instead $I_{MB} = I_{MB}(Q^2)$, where Q^2 measures the resolving scale of any probe and $I_{MB}(Q^2) \to 0^+$ monotonically with increasing Q^2. Moreover, form factors in QCD possess power-law behavior, so it is appropriate to renormalize the dressed-quark-core contributions via the estimate

$$F_{\rm core}(Q^2) \to [1 - I_{MB}(Q^2)] F_{\rm core}(Q^2), \tag{5.6a}$$

$$I_{MB}(Q^2) = [1 - 0.8^2]/[1 + Q^2/\Lambda_{MB}^2], \tag{5.6b}$$

with $\Lambda_{MB} = 1$ GeV marking the midpoint of the transition between the strong and perturbative domains of QCD as measured by the behavior of the dressed-quark mass function in Fig. 14. Following this procedure (Roberts and Segovia, 2016), one arrives at the estimate of MB FSI contributions depicted in Fig. 16.

The lower panel of Fig. 16 depicts the Pauli form factor F_2^*. All observations made regarding F_1^* also apply here, including those concerning the inferred meson-cloud contributions. Importantly, the existence of a zero in F_2^* is not influenced by meson-cloud effects, although its precise location is.

This is an opportune moment to review the picture of the Roper resonance that is painted by constituent-quark models. Figure 6 emphasized the importance of relativity in reproducing a zero in F_2^*, which generates the zero in $A_{1/2}$. And the discussion in this section has highlighted the fact that the natural degrees of freedom to employ when studying measurable form factors are strongly dressed quasiparticles (and correlations between them). It is interesting, therefore, that constituent-quark models, formulated using light-front quantization (LF CQMs) and incorporating aspects of the QCD dressing explained herein, have been used with success to describe features of the nucleon-Roper transition (Cardarelli *et al.*, 1997; Aznauryan and Burkert, 2012b, 2016). In these models, the dressing effects are implemented phenomenologically, i.e., via parametrizations chosen in order to secure a good fit to certain data, and they do not properly comply with QCD constraints at large momenta, e.g., using constituent-quark electromagnetic form factors that fall too quickly with increasing momentum transfer (Cardarelli *et al.*, 1997) or a dressed-quark mass function that falls too slowly (Aznauryan and Burkert, 2012b). Notwithstanding these limitations, the outcomes expressed are qualitatively significant. This is also illustrated in Fig. 16, which reveals a striking similarity between the DSE prediction for the dressed-quark-core components of the transition form factors and those computed using a LF CQM that incorporates a running quark mass (dotted, brown curve) (Aznauryan and Burkert, 2016). The parameters of the LF CQM model were adjusted by fitting nucleon elastic form factors on $Q^2 \in [0, 16]$ GeV^2, allowing room for MB FSIs and estimating their impact. Qualitatively, therefore, despite fundamental differences in formulation, both the DSE and LF CQM approaches arrive at the same conclusion regarding the nature of the proton-Roper transition form factors: while MB FSIs contribute materially on $x \lesssim 2$, a dressed-quark core is exposed and probed on $x \gtrsim 2$.

It should be emphasized here that were the Roper a purely molecular meson-baryon system, in the sense defined in Sec. IV, then the transition form factors would express an overlap between an initial-state proton, which certainly possesses a dressed-quark core, and a far more diffuse system. In such circumstances, $F_{1,2}^*$ would be much softer than anything that could be produced by a final state with a material dressed-quark core. However, Fig. 16 reveals that the extracted transition form factors are hard, explained by scattering from a three-valence-quark system on $x \gtrsim 2$. In addition, as described in Sec. III, one now has experimental results on $N\pi$ and $\pi^+\pi^- p$ electroproduction off protons in 21 Q^2 bins, covering the range $[0.2, 4.5]$ GeV^2; and they are uniformly described by a unique Roper resonance mass and total and partial hadronic decay widths that are Q^2 independent. Together, these observations render a purely molecular hypothesis untenable.

Finally, given the scope of agreement between experiment and theory in Fig. 16, one should apply a final test, viz. does the same perspective also deliver a consistent description of the nucleon and Δ-baryon elastic form factors and the nucleon-Δ transition? An affirmative answer is supported by an array of results (Segovia, Cloët *et al.*, 2014; Roberts, 2015, 2018; Segovia and Roberts, 2016).

VI. CONCLUSION

After more than fifty years, a coherent picture connecting the Roper resonance with the nucleon's first radial excitation has become visible. Completing this portrait only became possible following: (i) the acquisition and analysis of a vast amount of high-precision nucleon-resonance electroproduction data with single- and double-pion final states on a large kinematic domain of energy and momentum transfer; (ii) development of a sophisticated dynamical reaction theory capable of simultaneously describing all partial waves extracted from available, reliable data; (iii) formulation, and wide-ranging application of a Poincaré covariant approach to the continuum bound-state problem in relativistic quantum field theory that expresses diverse local and global impacts of DCSB in QCD; and (iv) the refinement of constituent-quark models so that they, too, qualitatively incorporate these aspects of strong QCD. In this picture:

- The Roper resonance is, at heart, the first radial excitation of the nucleon.
- It consists of a well-defined dressed-quark core, which plays a role in determining the system's properties at all length scales, but exerts a dominant influence on probes with $Q^2 \gtrsim m_N^2$, where m_N is the nucleon mass.
- The core is augmented by a meson cloud, which both reduces the Roper's core mass by ≈20%, thereby solving the mass problem that was such a puzzle in constituent-quark model treatments, and, at low-Q^2, contributes an amount to the electroproduction transition form factors that is comparable in magnitude with that of the dressed-quark core, but vanishes rapidly as Q^2 is increased beyond m_N^2.

These fifty years of experience with the Roper resonance have delivered lessons that cannot be emphasized too strongly. Namely, in attempting to predict and explain the QCD spectrum, one must fully consider the impact of meson-baryon final-state interactions and the couplings between channels and states that they generate, and look beyond merely locating the poles in the S matrix, which themselves reveal little structural information, to also consider the Q^2 dependences of the residues, which serve as a penetrating scale-dependent probe of resonance composition.

Moreover, the Roper resonance is not unusual. Indeed, in essence, the picture drawn here is also applicable to the Δ baryon, and an accumulating body of experiment and theory indicates that almost all baryon resonances can be viewed the same way, viz. as systems possessing a three-body dressed-quark bound-state core that is supplemented by a meson cloud, whose importance varies from state to state and whose observable manifestations disappear rapidly as the resolving power of the probe is increased. In this connection, it is important to highlight that CLAS12 at the newly upgraded JLab will be capable of determining the electrocouplings of most prominent nucleon resonances at unprecedented photon virtualities $Q^2 \in [6, 12]$ GeV^2 (Gothe *et al.*, 2009; Carman *et al.*, 2014). Consequently, the associated experimental program will be a powerful means of validating the perspective described herein.

Assuming the picture we have drawn is correct, then CLAS12 will deliver empirical information that can address a wide range of issues that are critical to our understanding of strong interactions (Burkert, 2018), e.g., is there an environment sensitivity of DCSB, and are quark-quark correlations an essential element in the structure of all baryons? As reviewed herein, existing experiment-theory feedback suggests that there is no environment sensitivity for the nucleon, Δ baryon, and Roper resonance: DCSB in these systems is expressed in ways that can readily be predicted once its manifestation is understood in the pion, and this includes the generation of diquark correlations with the same character in each of these baryons. Resonances in other channels, however, may contain additional diquark correlations, with different quantum numbers, and potentially be influenced in new ways by MB FSIs. Therefore, these channels, and higher excitations, open new windows on sQCD and its emergent phenomena whose vistas must be explored and mapped if the most difficult part of the standard model is finally to be solved.

ACKNOWLEDGMENTS

In preparing this article we benefited greatly from constructive comments and input provided by I. G. Aznauryan, A. Bashir, D. Binosi, L. Chang, C. Chen, Z.-F. Cui, B. El-Bennich, R. Gothe, L. X. Gutiérrez-Guerrero, G. Krein, T.-S. H. Lee, H.-W. Lin, K.-F. Liu, Y. Lu, C. Mezrag, V. Mokeev, J. Papavassiliou, J.-L. Ping, H. L. L. Roberts, J. Rodrigíuez-Quintero, T. Sato, S. M. Schmidt, J. Segovia, F. Wang, D. J. Wilson, S.-S. Xu, and H.-S. Zong. This work was supported by U.S. Department of Energy, Office of Science, Office of Nuclear Physics, under Contracts No. DE-AC05-06OR23177 and No. DE-AC02-06CH11357.

REFERENCES

Aaij, R., *et al.*, 2015, Phys. Rev. Lett. **115**, 072001.
Abbott, L. F., 1981, Nucl. Phys. B **185**, 189.
Abbott, L. F., 1982, Acta Phys. Pol. B **13**, 33 [http://inspirehep.net/record/166273/files/v13p0033.pdf].
Abe, K., *et al.*, 1995a, Phys. Lett. B **364**, 61.
Abe, K., *et al.*, 1995b, Phys. Rev. Lett. **75**, 25.
Abe, K., *et al.*, 1995c, Phys. Rev. Lett. **74**, 346.
Abe, K., *et al.*, 1996, Phys. Rev. Lett. **76**, 587.
Abe, K., *et al.*, 1997a, Phys. Lett. B **404**, 377.
Abe, K., *et al.*, 1997b, Phys. Lett. B **405**, 180.
Abe, K., *et al.*, 1997c, Phys. Rev. Lett. **79**, 26.
Abe, K., *et al.*, 1998, Phys. Rev. D **58**, 112003.
Ackerstaff, K., *et al.*, 1997, Phys. Lett. B **404**, 383.
Ackerstaff, K., *et al.*, 1998, Phys. Lett. B **444**, 531.
Adelman, S. L., 1964, Phys. Rev. Lett. **13**, 555.
Adolph, C., *et al.*, 2016, Phys. Lett. B **753**, 18.

Aguilar, A. C., D. Binosi, and J. Papavassiliou, 2016, Front. Phys. **11**, 111203.

Airapetian, A., *et al.*, 1998, Phys. Lett. B **442**, 484.

Airapetian, A., *et al.*, 2003, Phys. Rev. Lett. **90**, 092002.

Airapetian, A., *et al.*, 2007, Phys. Rev. D **75**, 012007.

Alekseev, M. G., *et al.*, 2010, Phys. Lett. B **690**, 466.

Alexakhin, V. Yu., *et al.*, 2007, Phys. Lett. B **647**, 8.

Alexandrou, C., Ph. de Forcrand, and B. Lucini, 2006, Phys. Rev. Lett. **97**, 222002.

Alexandrou, C., T. Leontiou, C. N. Papanicolas, and E. Stiliaris, 2015, Phys. Rev. D **91**, 014506.

Altarelli, G., and G. Parisi, 1977, Nucl. Phys. B **126**, 298.

Anisovich, A. V., *et al.*, 2017, Phys. Rev. Lett. **119**, 062004.

Anthony, P. L., *et al.*, 1993, Phys. Rev. Lett. **71**, 959.

Anthony, P. L., *et al.*, 1996, Phys. Rev. D **54**, 6620.

Anthony, P. L., *et al.*, 1999a, Phys. Lett. B **463**, 339.

Anthony, P. L., *et al.*, 1999b, Phys. Lett. B **458**, 529.

Anthony, P. L., *et al.*, 2000, Phys. Lett. B **493**, 19.

Anthony, P. L., *et al.*, 2003, Phys. Lett. B **553**, 18.

Arndt, R. A., W. J. Briscoe, I. I. Strakovsky, and R. L. Workman, 2006, Phys. Rev. C **74**, 045205.

Arndt, R. A., J. M. Ford, and L. D. Roper, 1985, Phys. Rev. D **32**, 1085.

Auvil, P., C. Lovelace, A. Donnachie, and A. Lea, 1964, Phys. Lett. **12**, 76.

Aznauryan, I., and V. Burkert, 2012a, Prog. Part. Nucl. Phys. **67**, 1.

Aznauryan, I., and V. Burkert, 2012b, Phys. Rev. C **85**, 055202.

Aznauryan, I., *et al.*, 2009, Phys. Rev. C **80**, 055203.

Aznauryan, I. G., 2003, Phys. Rev. C **67**, 015209.

Aznauryan, I. G., and V. D. Burkert, 2016, "Configuration mixings and light-front relativistic quark model predictions for the electro-excitation of the $\Delta(1232)3/2^+$, $N(1440)1/2^+$, and $\Delta(1600)3/2^+$," arXiv:1603.06692.

Aznauryan, I. G., V. D. Burkert, H. Egiyan, K. Joo, R. Minehart, and L. C. Smith, 2005, Phys. Rev. C **71**, 015201.

Aznauryan, I. G., *et al.*, 2008, Phys. Rev. C **78**, 045209.

Babich, R., N. Garron, C. Hoelbling, J. Howard, L. Lellouch, and Claudio Rebbi, 2007, Phys. Rev. D **76**, 074021.

Ball, J. S., and T.-W. Chiu, 1980, Phys. Rev. D **22**, 2542.

Bareyre, P., C. Bricman, G. Valladas, G. Villet, J. Bizard, and J. Seguinot, 1964, Phys. Lett. **8**, 137.

Barnes, T., and F. E. Close, 1983, Phys. Lett. B **123**, 89.

Bashir, A., *et al.*, 2012, Commun. Theor. Phys. **58**, 79.

Bender, A., W. Detmold, C. D. Roberts, and A. W. Thomas, 2002, Phys. Rev. C **65**, 065203.

Bender, A., C. D. Roberts, and L. von Smekal, 1996, Phys. Lett. B **380**, 7.

Bhagwat, M. S., A. Höll, A. Krassnigg, C. D. Roberts, and P. C. Tandy, 2004, Phys. Rev. C **70**, 035205.

Bhagwat, M. S., M. A. Pichowsky, C. D. Roberts, and P. C. Tandy, 2003, Phys. Rev. C **68**, 015203.

Bhagwat, M. S., and P. C. Tandy, 2006, AIP Conf. Proc. **842**, 225.

Bijker, R., and E. Santopinto, 2009, Phys. Rev. C **80**, 065210.

Binosi, D., L. Chang, J. Papavassiliou, S.-X. Qin, and C. D. Roberts, 2017, Phys. Rev. D **95**, 031501(R).

Binosi, D., L. Chang, J. Papavassiliou, and C. D. Roberts, 2015, Phys. Lett. B **742**, 183.

Binosi, D., C. Mezrag, J. Papavassiliou, C. D. Roberts, and J. Rodríguez-Quintero, 2017, Phys. Rev. D **96**, 054026.

Binosi, D., and J. Papavassiliou, 2002, Phys. Rev. D **66**, 111901.

Binosi, D., and J. Papavassiliou, 2004, J. Phys. G **30**, 203.

Binosi, D., and J. Papavassiliou, 2009, Phys. Rep. **479**, 1.

Bohr, N., 1913, Philos. Mag. **26**, 1.

Boucaud, P., J. P. Leroy, A. Le-Yaouanc, J. Micheli, O. Pene, and J. Rodríguez-Quintero, 2012, Few-Body Syst. **53**, 387.

Bowman, P. O., *et al.*, 2005, Phys. Rev. D **71**, 054507.

Braaten, E., 2016, Eur. Phys. J. Web Conf. **113**, 01015.

Briceno, R. A., J. J. Dudek, and R. D. Young, 2018, Rev. Mod. Phys. **90**, 025001.

Brodsky, S. J., A. L. Deshpande, H. Gao, R. D. McKeown, C. A. Meyer, Z.-E. Meziani, R. G. Milner, J.-W. Qiu, D. G. Richards, and C. D. Roberts, 2015, "QCD and Hadron Physics," arXiv:1502.05728.

Burden, C. J., R. T. Cahill, and J. Praschifka, 1989, Aust. J. Phys. **42**, 147.

Burkert, V. D., 2012, Eur. Phys. J. Web Conf. **37**, 01017.

Burkert, V. D., 2018, Annu. Rev. Nucl. Part. Sci. **68**, 405.

Burkert, V. D., and T. S. H. Lee, 2004, Int. J. Mod. Phys. E **13**, 1035.

Cahill, R. T., 1989, Aust. J. Phys. **42**, 171.

Cahill, R. T., C. D. Roberts, and J. Praschifka, 1987, Phys. Rev. D **36**, 2804.

Cahill, R. T., C. D. Roberts, and J. Praschifka, 1989, Aust. J. Phys. **42**, 129.

Cano, F., and P. Gonzalez, 1998, Phys. Lett. B **431**, 270.

Capstick, S., and N. Isgur, 1986, Phys. Rev. D **34**, 2809.

Capstick, S., and B. D. Keister, 1995, Phys. Rev. D **51**, 3598.

Capstick, S., and P. R. Page, 2002, Phys. Rev. C **66**, 065204.

Capstick, S., and W. Roberts, 2000, Prog. Part. Nucl. Phys. **45**, S241.

Cardarelli, F., E. Pace, G. Salme, and S. Simula, 1997, Phys. Lett. B **397**, 13.

Carman, D. S., *et al.*, 2014, "Exclusive $N^* \to KY$ Studies with CLAS12," JLab 12 Experiment E12-06-108A.

Caso, C., *et al.*, 1998, Eur. Phys. J. C **3**, 1.

Chang, L., I. C. Cloët, B. El-Bennich, T. Klähn, and C. D. Roberts, 2009, Chin. Phys. C **33**, 1189.

Chang, L., C. D. Roberts, and S. M. Schmidt, 2013, Phys. Rev. C **87**, 015203.

Chang, L., C. D. Roberts, and P. C. Tandy, 2011, Chin. J. Phys. **49**, 955 [https://www.ps-taiwan.org/cjp/download.php?type=paper&vol;=49#=5&page;=955].

Chen, C., B. El-Bennich, C. D. Roberts, S. M. Schmidt, J. Segovia, and S. Wan, 2018, Phys. Rev. D **97**, 034016.

Chen, X., J. Ping, C. D. Roberts, and J. Segovia, 2018, Phys. Rev. D **97**, 094016.

Cloët, I. C., and C. D. Roberts, 2008, *Proc. Sci.* LC2008, 047.

Cloët, I. C., C. D. Roberts, and A. W. Thomas, 2013, Phys. Rev. Lett. **111**, 101803.

Close, F. E., and Z.-P. Li, 1990, Phys. Rev. D **42**, 2194.

Cornwall, J. M., 1982, Phys. Rev. D **26**, 1453.

Cornwall, J. M., and J. Papavassiliou, 1989, Phys. Rev. D **40**, 3474.

Crede, V., and W. Roberts, 2013, Rep. Prog. Phys. **76**, 076301.

Cutkosky, R. E., and S. Wang, 1990, Phys. Rev. D **42**, 235.

Cyrol, A. K., L. Fister, M. Mitter, J. M. Pawlowski, and N. Strodthoff, 2016, Phys. Rev. D **94**, 054005.

Dalitz, R., and R. Moorhouse, 1965, Phys. Lett. **14**, 159.

Deur, A., V. Burkert, J.-P. Chen, and W. Korsch, 2007, Phys. Lett. B **650**, 244.

Deur, A., V. Burkert, J.-P. Chen, and W. Korsch, 2008, Phys. Lett. B **665**, 349.

Deur, A., Y. Prok, V. Burkert, D. Crabb, F. X. Girod, K. A. Griffioen, N. Guler, S. E. Kuhn, and N. Kvaltine, 2014, Phys. Rev. D **90**, 012009.

Dirac, P. A. M., 1928, Proc. R. Soc. A **117**, 610.

Dokshitzer, Y. L., 1977, Sov. Phys. JETP **46**, 641 [http://inspirehep.net/record/126153?ln=en].

Döring, M., 2014, Int. J. Mod. Phys. Conf. Ser. **26**, 1460054.

Döring, M., C. Hanhart, F. Huang, S. Krewald, and U. G. Meissner, 2009, Nucl. Phys. A **829**, 170.

Drechsel, D., O. Hanstein, S. S. Kamalov, and L. Tiator, 1999, Nucl. Phys. A **645**, 145.

Drechsel, D., S. S. Kamalov, and L. Tiator, 2007, Eur. Phys. J. A **34**, 69.

Dugger, M., *et al.*, 2009, Phys. Rev. C **79**, 065206.

Durr, S., *et al.*, 2008, Science **322**, 1224.

Edwards, R. G., J. J. Dudek, D. G. Richards, and S. J. Wallace, 2011, Phys. Rev. D **84**, 074508.

Efimov, G. V., M. A. Ivanov, and V. E. Lyubovitskij, 1990, Z. Phys. C **47**, 583.

Efremov, A. V., and A. V. Radyushkin, 1980, Phys. Lett. B **94**, 245.

Eichmann, G., R. Alkofer, I. C. Cloët, A. Krassnigg, and C. D. Roberts, 2008, Phys. Rev. C **77**, 042202(R).

Eichmann, G., R. Alkofer, A. Krassnigg, and D. Nicmorus, 2010, Phys. Rev. Lett. **104**, 201601.

Eichmann, G., I. C. Cloët, R. Alkofer, A. Krassnigg, and C. D. Roberts, 2009, Phys. Rev. C **79**, 012202(R).

Eichmann, G., C. S. Fischer, and H. Sanchis-Alepuz, 2016, Phys. Rev. D **94**, 094033.

Eichmann, G., H. Sanchis-Alepuz, R. Williams, R. Alkofer, and C. S. Fischer, 2016, Prog. Part. Nucl. Phys. **91**, 1.

Eidelman, S., *et al.*, 2004, Phys. Lett. B **592**, 1.

Engel, G. P., C. Lang, D. Mohler, and A. Schäfer, 2013, Phys. Rev. D **87**, 074504.

Feynman, R. P., 1966, Science **153**, 699.

Gao, F., L. Chang, Y.-X. Liu, C. D. Roberts, and P. C. Tandy, 2017, Phys. Rev. D **96**, 034024.

Gattringer, C., and C. B. Lang, 2010, Lect. Notes Phys. **788**, 1.

Geiger, H., and E. Marsden, 1909, Proc. R. Soc. A **82**, 495.

Gell-Mann, M., 1964, Phys. Lett. **8**, 214.

Gell-Mann, M., and F. E. Low, 1954, Phys. Rev. **95**, 1300.

Gerhardt, C., 1980, Z. Phys. C **4**, 311.

Giannini, M. M., and E. Santopinto, 2015, Chin. J. Phys. **53**, 020301.

Glozman, L. Ya., and D. O. Riska, 1996, Phys. Rep. **268**, 263.

Godfrey, S., and N. Isgur, 1985, Phys. Rev. D **32**, 189.

Gothe, R. W., *et al.*, 2009, "Nucleon Resonance Studies with CLAS12," jLab 12 Experiment E12-09-003.

Greenberg, O. W., 1964, Phys. Rev. Lett. **13**, 598.

Gribov, V. N., and L. N. Lipatov, 1972, Sov. J. Nucl. Phys. **15**, 438 [http://inspirehep.net/record/73449?ln=en].

Gromes, D., and I. O. Stamatescu, 1976, Nucl. Phys. B **112**, 213.

Gross, D., 2005, Proc. Natl. Acad. Sci. U.S.A. **102**, 9099.

Grunberg, G., 1984, Phys. Rev. D **29**, 2315.

Hecht, M. B., C. D. Roberts, M. Oettel, A. W. Thomas, S. M. Schmidt, and P. C. Tandy, 2002, Phys. Rev. C **65**, 055204.

Hey, A. J. G., and R. L. Kelly, 1983, Phys. Rep. **96**, 71.

Høgaasen, H., and J. M. Richard, 1983, Phys. Lett. B **124**, 520.

Höll, A., A. Krassnigg, and C. D. Roberts, 2004, Phys. Rev. C **70**, 042203(R).

Horn, T., and C. D. Roberts, 2016, J. Phys. G **43**, 073001.

Isgur, N., 2000, in "Newport News 2000, Excited nucleons and hadronic structure," pp. 403–422, arXiv:nucl-th/0007008v1.

Isgur, N., and G. Karl, 1979, Phys. Rev. D **19**, 2653; [**23**, 817(E) 1981)].

Ishii, N., 1998, Phys. Lett. B **431**, 1.

Isupov, E. L., *et al.*, 2017, Phys. Rev. C **96**, 025209.

Julia-Diaz, B., T. S. H. Lee, A. Matsuyama, and T. Sato, 2007, Phys. Rev. C **76**, 065201.

Julia-Diaz, B., and D. Riska, 2006, Nucl. Phys. A **780**, 175.

Kamano, H., and T. S. H. Lee, 2012, AIP Conf. Proc. **1432**, 74.

Kamano, H., S. X. Nakamura, T. S. H. Lee, and T. Sato, 2010, Phys. Rev. C **81**, 065207.

Kamano, H., S. X. Nakamura, T. S. H. Lee, and T. Sato, 2013, Phys. Rev. C **88**, 035209.

Kaulfuss, U. B., and U. G. Meissner, 1985, Phys. Lett. B **154**, 193.

Kim, J. H., *et al.*, 1998, Phys. Rev. Lett. **81**, 3595.

Koniuk, R., and N. Isgur, 1980, Phys. Rev. D **21**, 1868; [**23**, 818(E) 1981)].

Lamb, W. E., and R. C. Retherford, 1947, Phys. Rev. **72**, 241.

Lee, T. S. H., 2007, J. Phys. Conf. Ser. **69**, 012013.

Lee, T. S. H., 2013, AIP Conf. Proc. **1560**, 413.

Lepage, G. P., and S. J. Brodsky, 1979, Phys. Lett. B **87**, 359.

Lepage, G. P., and S. J. Brodsky, 1980, Phys. Rev. D **22**, 2157.

Li, Z.-p., V. Burkert, and Z.-j. Li, 1992, Phys. Rev. D **46**, 70.

Lichtenberg, D. B., and L. J. Tassie, 1967, Phys. Rev. **155**, 1601.

Lichtenberg, D. B., L. J. Tassie, and P. J. Keleman, 1968, Phys. Rev. **167**, 1535.

Lin, H.-W., and S. D. Cohen, 2012, AIP Conf. Proc. **1432**, 305.

Lin, H.-W., S. D. Cohen, R. G. Edwards, and D. G. Richards, 2008, Phys. Rev. D **78**, 114508.

Liu, K.-F., 2017, Int. J. Mod. Phys. E **26**, 1740016.

Liu, K.-F., Y. Chen, M. Gong, R. Sufian, M. Sun, and A. Li, 2014, *Proc. Sci.* LATTICE2013, 507.

Löring, U., B. C. Metsch, and H. R. Petry, 2001, Eur. Phys. J. A **10**, 395.

Lu, Y., C. Chen, C. D. Roberts, J. Segovia, S.-S. Xu, and H.-S. Zong, 2017, Phys. Rev. C **96**, 015208.

Mahbub, M. S., W. Kamleh, D. B. Leinweber, P. J. Moran, and A. G. Williams, 2012, Phys. Lett. B **707**, 389.

Marciano, W. J., and H. Pagels, 1978, Phys. Rep. **36**, 137.

Marciano, W. J., and H. Pagels, 1979, Nature (London) **279**, 479.

Maris, P., 2002, Few-Body Syst. **32**, 41.

Maris, P., 2004, Few-Body Syst. **35**, 117.

Maris, P., C. D. Roberts, and P. C. Tandy, 1998, Phys. Lett. B **420**, 267.

Matsuyama, A., T. Sato, and T. S. H. Lee, 2007, Phys. Rep. **439**, 193.

Mattis, M. P., and M. Karliner, 1985, Phys. Rev. D **31**, 2833.

Mokeev, V. I., I. Aznauryan, V. Burkert, and R. Gothe, 2016, Eur. Phys. J. Web Conf. **113**, 01013.

Mokeev, V. I., *et al.*, 2012, Phys. Rev. C **86**, 035203.

Mokeev, V. I., *et al.*, 2016, Phys. Rev. C **93**, 025206.

Moorhouse, R. G., 1966, Phys. Rev. Lett. **16**, 772.

Nambu, Y., 2011, AIP Conf. Proc. **1388**, 86.

Pilaftsis, A., 1997, Nucl. Phys. B **487**, 467.

Politzer, H. D., 2005, Proc. Natl. Acad. Sci. U.S.A. **102**, 7789.

Qin, S.-X., L. Chang, Y.-X. Liu, C. D. Roberts, and D. J. Wilson, 2012, Phys. Rev. C **85**, 035202.

Raya, K., L. Chang, A. Bashir, J. J. Cobos-Martinez, L. X. Gutiérrez-Guerrero, C. D. Roberts, and P. C. Tandy, 2016, Phys. Rev. D **93**, 074017.

Reinhardt, H., 1990, Phys. Lett. B **244**, 316.

Richard, J. M., 1992, Phys. Rep. **212**, 1.

Ripani, M., *et al.*, 2003, Phys. Rev. Lett. **91**, 022002.

Roberts, C. D., 2015, J. Phys. Conf. Ser. **630**, 012051.

Roberts, C. D., 2016, J. Phys. Conf. Ser. **706**, 022003.

Roberts, C. D., 2017, Few-Body Syst. **58**, 5.

Roberts, C. D., 2018, Few-Body Syst. **59**, 72.

Roberts, C. D., R. J. Holt, and S. M. Schmidt, 2013, Phys. Lett. B **727**, 249.

Roberts, C. D., and J. Segovia, 2016, Few-Body Syst. **57**, 1067.

Roberts, C. D., and A. G. Williams, 1994, Prog. Part. Nucl. Phys. **33**, 477.

Roberts, D. S., W. Kamleh, and D. B. Leinweber, 2013, Phys. Lett. B **725**, 164.

Roberts, H. L. L., A. Bashir, L. X. Gutiérrez-Guerrero, C. D. Roberts, and D. J. Wilson, 2011, Phys. Rev. C **83**, 065206.

Rojas, E., B. El-Bennich, and J. P. B. C. de Melo, 2014, Phys. Rev. D **90**, 074025.
Rönchen, D., Döring, M., F. Huang, H. Haberzettl, J. Haidenbauer, C. Hanhart, S. Krewald, U. G. Meissner, and K. Nakayama, 2013, Eur. Phys. J. A **49**, 44.
Roper, L. D., 1964, Phys. Rev. Lett. **12**, 340.
Roper, L. D., R. M. Wright, and B. T. Feld, 1965, Phys. Rev. **138**, B190.
Rutherford, E., 1911, Philos. Mag. **21**, 669.
Sanchis-Alepuz, H., C. S. Fischer, and S. Kubrak, 2014, Phys. Lett. B **733**, 151.
Sato, T., and T. S. H. Lee, 1996, Phys. Rev. C **54**, 2660.
Schwinger, J. S., 1982, J. Phys. (Paris), Colloq. **43**, C8-409.
Segovia, J., C. Chen, I. C. Cloët, C. D. Roberts, S. M. Schmidt, and S.-L. Wan, 2014, Few-Body Syst. **55**, 1.
Segovia, J., I. C. Cloët, C. D. Roberts, and S. M. Schmidt, 2014, Few-Body Syst. **55**, 1185.
Segovia, J., B. El-Bennich, E. Rojas, I. C. Cloët, C. D. Roberts, S.-S. Xu, and H.-S. Zong, 2015, Phys. Rev. Lett. **115**, 171801.
Segovia, J., and C. D. Roberts, 2016, Phys. Rev. C **94**, 042201(R).
Segovia, J., C. D. Roberts, and S. M. Schmidt, 2015, Phys. Lett. B **750**, 100.
Shen, C.-P., 2016, Eur. Phys. J. Web Conf. **113**, 01016.
Štajner, S., *et al.*, 2017, Phys. Rev. Lett. **119**, 022001.
Suzuki, N., B. Julia-Diaz, H. Kamano, T. S. H. Lee, A. Matsuyama, and T. Sato, 2010, Phys. Rev. Lett. **104**, 042302.
Tanabashi, M., *et al.*, 2018, Phys. Rev. D **98**, 030001.
Tiator, L., D. Drechsel, S. Kamalov, M. M. Giannini, E. Santopinto, and A. Vassallo, 2004, Eur. Phys. J. A **19**, 55.
Tomonaga, S.-i., 1966, Phys. Today **19**, No. 9, 25.
Warns, M., H. Schroder, W. Pfeil, and H. Rollnik, 1990, Z. Phys. C **45**, 627.
Wilczek, F., 2000, Phys. Today **53**, No. 8, 22.
Wilczek, F., 2005, Proc. Natl. Acad. Sci. U.S.A. **102**, 8403.
Wilczek, F., 2012, Central Eur. J. Phys. **10**, 1021.
Wilson, D. J., I. C. Cloët, L. Chang, and C. D. Roberts, 2012, Phys. Rev. C **85**, 025205.
Wilson, K. G., 1974, Phys. Rev. D **10**, 2445.
Xu, S.-S., C. Chen, I. C. Cloët, C. D. Roberts, J. Segovia, and H.-S. Zong, 2015, Phys. Rev. D **92**, 114034.
Zweig, G., 1964, "An $SU(3)$ model for strong interaction symmetry and its breaking, Parts 1 and 2," CERN Reports No. 8182/TH. 401 and No. 8419/TH. 412).